Goal-oriented *h*-adaptivity for the Helmholtz equation: error estimates, local indicators and refinement strategies

Lindaura Maria Steffens · Núria Parés · Pedro Díez

Abstract This paper introduces a new goal-oriented adaptive technique based on a simple and effective post-process of the finite element approximations. The goal-oriented character of the estimate is achieved by analyzing both the direct problem and an auxiliary problem, denoted as *adjoint* or *dual* problem, which is related to the quantity of interest. Thus, the error estimation technique proposed in this paper would fall into the category of recovery-type explicit residual *a posteriori* error estimates. The procedure is valid for general linear quantities of interest and it is also extended to non-linear ones. The numerical examples demonstrate the efficiency of the proposed approach and discuss: (1) different error representations, (2) assessment of the dispersion error, and (3) different remeshing criteria.

Keywords Goal-oriented adaptivity · Quantity of interest · Error estimates · Helmholtz equation · Dispersion error

1 Introduction

One of the major problems in acoustic simulations, and in particular in problems governed by the Helmholtz equation, is that the Galerkin method requires too fine meshes. This is computationally unaffordable and undermines the practical utility of the method. Often the *rule of the thumb*, which prescribes the minimal discretization per wavelength, is used. However, it is widely known that this rule is not sufficient to obtain reliable results for large wave numbers due to dispersion and pollution errors [1–5]. Furthermore, non-uniform meshes are required to resolve singularities or large gradients in the solution. This suggests using adaptivity to control the accuracy and obtain *optimal* meshes refining at the right locations.

The basic scheme of the adaptive procedure is: first, estimate the discretization error; second, develop the strategy associated with the *h*-adaptive refinement, which determines the elements to be refined; and finally, generate a new mesh. Obviously, the most important ingredient in any adaptive procedure is a reliable error estimation procedure.

Goal-oriented adaptivity is related with controlling the error in a given quantity of interest, and optimal refinement techniques should only refine the areas affecting this quantity. Moreover, the error assessment techniques for quantities of interest should provide both an approximation to the total error in the quantity of interest and also the local contributions of each element to the total error. These local quantities are used to design the adaptive procedure.

While some progress has been done in assessing the global accuracy of finite element approximations for the Helmholtz equation [6–10], there exist very few literature concerning a posteriori goal-oriented error estimation in this context [11–14]. For instance, [12] provides a strategy to compute asymptotic bounds for linear and non-linear quantities of interest based on the equilibrated residual method. Another example is [13] which proposes a goal-oriented adaptive technique for modeling the external human auditory system by the boundary element method.

The assessment of the quality of the finite element approximations of the Helmholtz equation is an important issue in acoustic computations. Recall that the transient wave equation reduces to the steady-state Helmholtz equation under the assumption of a time harmonic behavior of the solution. The solution of the transient wave equation is eventually recovered composing the solutions of the Helmholtz equation for

L. M. Steffens (✉) · N. Parés · P. Díez
Laboratori de Càlcul Numèric,
Departament de Matemàtica Aplicada III,
Universitat Politècnica de Catalunya, Barcelona, Spain
e-mail: lindaura.steffens@upc.edu

different frequencies ω. Thus, practical acoustic simulations require to solve the Helmholtz equation for a wide range of frequencies. In this context, the numerical solution of the Helmholtz equation requires a proper use of error control and adaptivity. This allows efficiently computing accurate solutions and saving computational resources in a process that has to be repeated a large number of times, for different frequencies.

The present work is concerned with obtaining accurate solutions of the Helmholtz equation for a given frequency ω. A major challenge in the field of error estimation, not addressed in here and still an open problem, is obtaining a goal-oriented error estimation strategy valid not only for specific values of the frequency but also for a range of frequencies. Note that finding the resonant frequencies of the problem or the study of dynamic instability phenomena is also beyond the scope of this paper.

The remainder of the paper is structured as follows: Sect. 2 introduces the description of the problem to be solved. Section 3 presents a general framework for assessing the error in general linear and non-linear quantities of interest. Different representations for the linear contribution to the output are introduced in Sect. 4. Section 5 is devoted to obtain error estimates for general outputs using the different error representations given in Sect. 4. The adaptive strategy is introduced in Sect. 6, where local indicators and several strategies of refinement are defined. Finally, in Sect. 7 the proposed procedure for goal-oriented adaptivity is tested in some numerical examples. The relation between the different error representations and the dispersion error of the direct and adjoint problems is also discussed.

2 Problem statement

The propagation of acoustic waves is governed by the wave equation describing the evolution of the acoustic pressure p as a function of the position $\mathbf{x}$ and time t. The harmonic assumption states that for a given angular frequency ω, $p(\mathbf{x}, t) = u(\mathbf{x})e^{i\omega t}$, where the new unknown $u(\mathbf{x})$ is the complex amplitude of the acoustic pressure. For an interior spatial domain Ω, $u(\mathbf{x})$ is the solution of the Helmholtz equation

$$-\Delta u - \kappa^2 u = f \quad \text{in } \Omega, \tag{1}$$

taking the acoustic wave number $\kappa = \omega/c$ where c is the speed of sound. In order to recover the solution of the transient wave problem, the Helmholtz equation has to be solved repeatedly for a range of wave numbers κ representing the spectrum of the waves appearing in the problem. Equation (1) is complemented with the following boundary conditions

$$u = u_D \quad \text{on } \Gamma_D, \tag{2a}$$

$$\nabla u \cdot \mathbf{n} = g \quad \text{on } \Gamma_N, \tag{2b}$$

$$\nabla u \cdot \mathbf{n} = mu + \beta \quad \text{on } \Gamma_R, \tag{2c}$$

where Γ_D, Γ_N and Γ_R are a disjoint partition of the boundary where Dirichlet, Neumann and Robin boundary conditions are applied respectively. The outward unit normal is denoted by $\mathbf{n}$ and u_D, f, g, m and β are the prescribed data, which are assumed to be sufficiently smooth.

The boundary value problem defined by Eqs. (1) and (2) is readily expressed in its weak form introducing the solution and test spaces $\mathscr{U} := \{u \in \mathscr{H}^1(\Omega), u|_{\Gamma_D} = u_D\}$ and $\mathscr{V} := \{v \in \mathscr{H}^1(\Omega), v|_{\Gamma_D} = 0\}$. Here $\mathscr{H}^1(\Omega)$ is the standard Sobolev space of complex-valued square integrable functions with square integrable first derivatives. The weak form of the problem then reads: find $u \in \mathscr{U}$ such that

$$a(u, v) = \ell(v) \quad \forall v \in \mathscr{V},$$

where the sesquilinear form $a(\cdot, \cdot)$ and antilinear functional $\ell(\cdot)$ are defined as

$$\begin{aligned} a(u, v) &:= \int_\Omega \nabla u \cdot \nabla \bar{v}\, d\Omega - \int_\Omega \kappa^2 u \bar{v}\, d\Omega - \int_{\Gamma_R} mu\bar{v}\, d\Gamma, \\ \ell(v) &:= \int_\Omega f\bar{v}\, d\Omega + \int_{\Gamma_N} g\bar{v}\, d\Gamma + \int_{\Gamma_R} \beta\bar{v}\, d\Gamma, \end{aligned} \tag{3}$$

and the symbol $\bar{\cdot}$ denotes the complex conjugate.

The finite element approximation of u is found by first discretizing the domain Ω into triangular or quadrilateral elements Ω_k, $k = 1, \ldots, \mathrm{n_{el}}$, $\mathrm{n_{el}}$ being the number of elements in the mesh. This mesh has an associated characteristic mesh size H and induces the discrete functional spaces $\mathscr{U}_H \subset \mathscr{U}$ and $\mathscr{V}_H \subset \mathscr{V}$. The finite element approximation $u_H \in \mathscr{U}_H$ is then such that

$$a(u_H, v) = \ell(v) \quad \forall v \in \mathscr{V}_H.$$

3 Error assessment for general (nonlinear) quantities of interest

A posteriori error estimation techniques aim at assessing the error committed in the approximation of u, $e := u - u_H$, where $e \in \mathscr{V}$ is the solution of the primal residual problem

$$a(e, v) = \ell(v) - a(u_H, v) =: R^P(v) \quad \forall v \in \mathscr{V}, \tag{4}$$

$R^P(\cdot)$ standing for the weak residual associated to the finite element approximation u_H.

When applied to classical problems (in which $a(\cdot, \cdot)$ is coercive) a first step in a posteriori assessment is estimating the error measured in the energy norm, that is obtaining a good approximation of e and computing $a(e, e)$. However, in acoustic problems, since the Helmholtz equation is not elliptic, the form $||v||^2 = a(v, v)$ does not define a

squared norm. There is no natural energy norm to measure the error.

Additionally, assessing the error measured in some functional norm is not sufficient for many applications. In practice, the finite element user is interested in specific magnitudes extracted from the global solution by some post-process. These magnitudes are referred to as quantities of interest or functional outputs. Goal-oriented error assessment strategies aim at estimating the error committed in these quantities and possibly providing bounds for it.

The quantities of interest considered here are nonlinear functional outputs of the solution, $J(u)$, and the aim is to assess the error committed when approximating these quantities using the finite element approximation. Specifically, the goal is to assess and control the quantity

$$J(u) - J(u_H).$$

For the purposes of this paper, it is convenient to make the linear, quadratic and higher order term contributions of $J(u)$ more explicit. To this end, $J(u)$ is expanded introducing the Gäteaux first and second derivatives of $J(\cdot)$ at u_H, namely

$$J(u_H + v) = J(u_H) + \ell^{\mathscr{O}}(v) + \mathscr{Q}(v, v) + \mathscr{W}(v), \qquad (5)$$

where $\ell^{\mathscr{O}}(v) = [D_v J](u_H)\cdot(v), 2\mathscr{Q}(v_1, v_2) = [D_v^2 J](u_H)\cdot(v_1, v_2)$, see [12,15], and the functional $\mathscr{W}$ contains the higher order terms.

Remark 1 As particular complex-valued functions, the forms $\ell^{\mathscr{O}} : \mathscr{H}^1(\Omega) \to \mathbb{C}$ and $\mathscr{Q} : \mathscr{H}^1(\Omega) \times \mathscr{H}^1(\Omega) \to \mathbb{C}$ are homogeneous of degree one and two respectively, in the sense that for any scalar value $\alpha \in \mathbb{R}$, $\ell^{\mathscr{O}}(\alpha v) = \alpha \ell^{\mathscr{O}}(v)$ and $\mathscr{Q}(\alpha v, \alpha v) = \alpha^2 \mathscr{Q}(v, v)$. For convenience, $\ell^{\mathscr{O}}(\cdot)$ and $\mathscr{Q}(\cdot, \cdot)$ are referred to as the linear and bilinear contributions of $J(\cdot)$ respectively, by analogy with the real-valued case. Note however that $\ell^{\mathscr{O}}(\cdot)$ being an homogeneous functional of degree one does not imply that it is a linear functional (it can be either linear, antilinear or a combination of both).

Henceforth, making an abuse of language which is unlikely to yield to confusion, the term linear is both used to denote a linear functional or mapping between two complex-valued spaces, like (7), and also to refer to the first Gâteaux derivative of the quantity of interest which is named after linear contribution or linear term.

In this respect, the usual statement of having a linear quantity of interest refers to $\mathscr{Q} = \mathscr{W} = 0$ in (5), where $\ell^{\mathscr{O}}(\cdot)$ is not necessarily a linear map (it may be partially antilinear).

Using this decomposition and taking into account that $u = u_H + e$, the error in the quantity of interest may be rewritten as

$$\begin{aligned} J(u) - J(u_H) &= J(u_H + e) - J(u_H) \\ &= \ell^{\mathscr{O}}(e) + \mathscr{Q}(e, e) + \mathscr{W}(e). \end{aligned} \qquad (6)$$

Thus, it is clear that in order to estimate the error in the quantity of interest, it is sufficient to estimate the linear, quadratic and higher-order terms separately, $\ell^{\mathscr{O}}(e)$, $\mathscr{Q}(e, e)$ and $\mathscr{W}(e)$ respectively.

Requiring $\mathscr{Q}$ and $\mathscr{W}$ to be $\mathscr{L}^2$-continuous, which in this particular case is equivalent to $|\mathscr{Q}(v, v)| \leq c_1 \|v\|^2$ and $|\mathscr{W}(v)| \leq c_2 \|v\|^3$ where $\|\cdot\|$ denotes the $\mathscr{L}^2$-norm, shows that the quadratic and higher-order contributions to the error, $\mathscr{Q}(e, e)$ and $\mathscr{W}(e)$, converge as $\mathscr{O}(H^4)$ and $\mathscr{O}(H^6)$ respectively, whereas the linear term $\ell^{\mathscr{O}}(e)$ converges quadratically—recall that the finite element method for a regular problem converges linearly in the $\mathscr{L}^2$-norm. Thus, for sufficiently small H the linear term provides a good inside to the error in the output since the other terms are negligible.

The following sections are devoted to describe the error assessment techniques to estimate $J(e)$ (linear and higher order contributions) and to provide local error estimators able to effectively drive the adaptive procedures.

4 Error representation of a linearized output and adjoint problem

This section presents alternative representations for the linear contribution to the error in the output $\ell^{\mathscr{O}}(e)$. These alternative representations do not directly yield computable expressions for the estimates of the output because they depend on the exact errors on the primal and adjoint problems. However, estimates may be easily recovered using existing techniques providing approximations for the errors, as described in the following section.

The quantities of interest considered here are such that their linear part is expressed as

$$\ell^{\mathscr{O}}(v) = \int_\Omega f^{\mathscr{O}} v \, d\Omega + \int_{\Gamma_N} g^{\mathscr{O}} v \, d\Gamma + \int_{\Gamma_R} \beta^{\mathscr{O}} v \, d\Gamma, \qquad (7)$$

where $f^{\mathscr{O}}$, $g^{\mathscr{O}}$ and $\beta^{\mathscr{O}}$ are given functions characterizing the linearized quantity of interest. Note that $\ell^{\mathscr{O}}(v)$ has the same structure as $\ell(v)$, see Eq. (4), excepting the conjugate in its argument. Thus, $\ell^{\mathscr{O}}(\cdot)$ is a linear functional whereas $\ell(\cdot)$ is an anti-linear functional.

Most existing techniques to estimate the error in a quantity of interest introduce an alternative representation for $\ell^{\mathscr{O}}(e)$. In practice, different error representations are used to properly estimate $\ell^{\mathscr{O}}(e)$. These error representations require introducing an auxiliary problem, denoted as *adjoint* or *dual* problem which reads: find $\psi \in \mathscr{V}$ such that

$$a(v, \psi) = \ell^{\mathscr{O}}(v) \quad \forall v \in \mathscr{V}, \qquad (8)$$

which is equivalent to determine the adjoint solution ψ verifying the Helmholtz equation

$$-\Delta\psi - \kappa^2\psi = \bar{f}^{\mathscr{O}} \quad \text{in } \Omega, \tag{9}$$

complemented with the boundary conditions

$$\psi = 0 \quad \text{on } \Gamma_D, \tag{10a}$$
$$\nabla\psi \cdot \mathbf{n} = \bar{g}^{\mathscr{O}} \quad \text{on } \Gamma_N, \tag{10b}$$
$$\nabla\psi \cdot \mathbf{n} = \bar{m}\psi + \bar{\beta}^{\mathscr{O}} \quad \text{on } \Gamma_R. \tag{10c}$$

Remark 2 It is worth noting that for a general nonlinear quantity of interest $J(u)$, its first Gâteaux derivative, expressed via the functional $\ell^{\mathscr{O}}(\cdot)$, is not necessarily of the form of (7). The proposed strategy is valid for general functionals $\ell^{\mathscr{O}}(\cdot)$. However if the linearized output $\ell^{\mathscr{O}}(\cdot)$ is not in the form of (7), the adjoint solution ψ is no longer the solution of the strong Helmholtz problem given by Eqs. (9) and (10), and the physical meaning of the adjoint solution may not be a clear cut. In some cases a simple workaround may be used to work with functionals of the preferred form (7), as will be seen in the numerical examples.

In order to assess the error in the quantity of interest the adjoint solution ψ is approximated numerically by $\psi_H \in \mathscr{V}_H$ such that

$$a(v, \psi_H) = \ell^{\mathscr{O}}(v) \quad \forall v \in \mathscr{V}_H,$$

introducing the adjoint error $\varepsilon := \psi - \psi_H$ solution of the adjoint residual problem

$$a(v, \varepsilon) = \ell^{\mathscr{O}}(v) - a(v, \psi_H) =: R^D(v) \quad \forall v \in \mathscr{V}_H, \tag{11}$$

where $R^D(\cdot)$ is the weak adjoint residual associated with ψ_H.

The adjoint problem is introduced such that the following error representation holds:

$$\ell^{\mathscr{O}}(e) = a(e, \psi) = a(e, \varepsilon)$$

where the Galerkin orthogonality of the adjoint approximation ψ_H is used in the last equality. In turn, this error representation allows assessing the error in terms of the residuals of the direct and adjoint problems, namely

$$\ell^{\mathscr{O}}(e) = a(e, \varepsilon) = R^P(\varepsilon) = R^D(e). \tag{12}$$

These representations are obtained substituting $v = \varepsilon$ in (4) and $v = e$ in (11) respectively.

5 Recovery type error estimates for linear and nonlinear outputs

A posteriori assessment of quantities of interest relies on obtaining a good approximation of $J(u) - J(u_H)$. This translates in finding a new enhanced solution u^*, based on the information at hand, that is u_H, and such that u^* approximates the actual solution u much better than u_H. Thus, a computable error estimate is readily obtained

$$e \approx e^* = u^* - u_H$$

yielding also the corresponding estimate for the quantity of interest

$$J(u) - J(u_H) \approx \ell^{\mathscr{O}}(e^*) + \mathscr{Q}(e^*, e^*) + \mathscr{W}(e^*). \tag{13}$$

This approximation of the error in the quantity of interest is obtained from Eq. (6) substituting the actual error e by its approximation e^*.

Thus, the key issue in any error estimation technique is to produce a properly enhanced solution u^* (or in some cases obtaining an enhanced approximation of the gradient of the solution $q^* \approx \nabla u$ suffices). The strategies producing the enhanced solution u^* (or q^* respectively) are classified into two categories: recovery type estimators and implicit residual type estimators. Recovery techniques, based on the ideas of Zienkiewicz and Zhu [16–18], are often preferred by practitioners because they are robust and simple to use. On the other hand, a posteriori implicit residual-type estimators have a sounder mathematical basis and produce estimates that are upper or lower bounds of the error [19–23]. At first glance on could think that, once the enhanced solutions u^* or q^* are obtained either using recovery or residual-type error estimators, estimates for the error in the quantity of interest may be directly obtained using Eq. (13). However, as mentioned in Sect. 4, this representation does not provide sound results. This is because inserting the enhanced error e^* (or its gradient q^*) in the functionals $\ell^{\mathscr{O}}(\cdot)$, $\mathscr{Q}(\cdot,\cdot)$ and $\mathscr{W}(\cdot)$ may not yield accurate results even when the enhanced approximation u^* provides a reasonable approximation of u in terms of energy. In practice, since the most-contributing term to the error in the quantity of interest is the linear term, alternative representations are used for this term, as the ones described in Sect. 4, whereas no additional effort is done in the higher-order terms.

The linear term $\ell^{\mathscr{O}}(e)$ may be assessed by any of the following strategies:

1. Compute the primal enhanced solution u^* to obtain $e^* = u^* - u_H$ and evaluate $\ell^{\mathscr{O}}(e^*)$. This option is readily discarded as announced previously.
2. Compute the primal enhanced solution u^* to obtain e^* and evaluate $R^D(e^*)$.
3. Compute the adjoint enhanced solution ψ^* to obtain $\varepsilon^* = \psi^* - \psi_H$ and evaluate $R^P(\varepsilon^*)$.
4. Compute both the primal and enhanced errors e^* and ε^* and evaluate $a(e^*, \varepsilon^*)$.

In this work, the strategies presented in [24,25] are used to recover the enhanced solutions u^* and ψ^* from u_H and

ψ_H respectively. A simple and inexpensive post-processing technique is used to recover the approximations u^* and ψ^* of u and ψ in a finer reference mesh of associated characteristic mesh size $h \ll H$. Thus, $u^* \in \mathscr{U}_h$ and $\psi^* \in \mathscr{V}_h$, where $\mathscr{U}_h$ and $\mathscr{V}_h$ are the discrete functional spaces associated to the finer reference mesh, $\mathscr{U}_H \subset \mathscr{U}_h \subset \mathscr{U}$ and $\mathscr{V}_H \subset \mathscr{V}_h \subset \mathscr{V}$.

As mentioned before, for sufficiently refined meshes, the error in the quantity of interest is controlled by the linear term, since the quadratic and higher-order contributions converge faster to zero, see Sect. 3. For this, the proposed approach is to make use of the available estimate e^* to obtain a simple and inexpensive estimate of the non-linear contributions. Namely, the quadratic and higher-order contributions to the error in the output, $\mathscr{Q}(e, e)$ and $\mathscr{W}(e)$ respectively, are assessed using the reconstruction of the primal error e^* used to assess the linear part of the error, namely

$$\mathscr{Q}(e, e) \approx \mathscr{Q}(e^*, e^*) \quad \text{and} \quad \mathscr{W}(e) \approx \mathscr{W}(e^*).$$

6 Local indicators and adaptivity criteria

Adaptive mesh refinement is nowadays an essential tool to obtain high-fidelity simulations at the lesser cost. The main ingredients of the proposed adaptive procedure are: the *h-refinement*, that is, the new meshes are obtained by subdividing the elements of the mesh; *optimal indicators*, the refinement is organized with the aim of achieving equal error in each element of the new mesh; *iterative process*, the target in each refinement step is to reduce the global error until the calculated error drops below the tolerance specified by the user.

Additionally, assessing the error measured in some functional norm is not sufficient for many applications. In practice, the finite element user is interested in specific magnitudes extracted from the global solution by some post-process. These magnitudes are referred to as quantities of interest or functional outputs. Goal-oriented error assessment strategies aim at estimating the error committed in these quantities and possibly providing bounds for it.

This requires obtaining local error indicators allowing to decide the elements to be marked for refinement—those with larger contribution to the total error. In order to determine the contribution of every element to the total error, spatial error distributions of the estimates are derived decomposing the global estimates into a sum of local contributions in each element of the mesh induced by $\mathscr{U}_H$.

The estimates for the error in the quantity of interest are of the form

$$J(u) - J(u_H) \approx \ell^{\mathscr{O}}(e^*) + \mathscr{Q}(e^*, e^*) + \mathscr{W}(e^*),$$

where the linear term $\ell^{\mathscr{O}}(e^*)$ is replaced by either $a(e^*, \varepsilon^*)$, $R^P(\varepsilon^*)$ or $R^D(e^*)$, depending on the selected representation of the linear term. Since the linear term is the driving term of the error in the quantity of interest, in this work, the adaptive procedure is chosen to be driven by $\ell^{\mathscr{O}}(e^*)$. That is, the global estimate for the linear term $\ell^{\mathscr{O}}(e^*)$ is decomposed into a sum of local contributions in each element. These local quantities are used to design the adaptive procedure.

6.1 Local indicators

The natural restriction to every element Ω_k of the integral forms $a(\cdot,\cdot)$, $\ell(\cdot)$ and $\ell^{\mathscr{O}}(\cdot)$ yield the elementary contributions denoted by $a_k(\cdot,\cdot)$, $\ell_k(\cdot)$ and $\ell_k^{\mathscr{O}}(\cdot)$ such that

$$a(u, v) = \sum_{k=1}^{\mathrm{n_{el}}} a_k(u, v), \quad \ell(v) = \sum_{k=1}^{\mathrm{n_{el}}} \ell_k(v),$$
$$\ell^{\mathscr{O}}(v) = \sum_{k=1}^{\mathrm{n_{el}}} \ell_k^{\mathscr{O}}(v).$$

Similarly, the primal and adjoint residuals are decomposed as

$$R^P(v) = \sum_{k=1}^{\mathrm{n_{el}}} R_k^P(v), \quad R^D(v) = \sum_{k=1}^{\mathrm{n_{el}}} R_k^D(v),$$

where $R_k^P(\cdot) := \ell_k(\cdot) - a_k(u_H, \cdot)$ and $R_k^D(\cdot) := \ell_k^{\mathscr{O}}(\cdot) - a_k(\cdot, \psi_H)$.

Hence, the error representations for the linear contribution of the error in the quantity of interest given in Eq. (12) are associated to the elementary error distributions

$$\ell^{\mathscr{O}}(e) = \sum_{k=1}^{\mathrm{n_{el}}} \ell_k^{\mathscr{O}}(e) = \sum_{k=1}^{\mathrm{n_{el}}} a_k(e, \varepsilon) = \sum_{k=1}^{\mathrm{n_{el}}} R_k^P(\varepsilon) = \sum_{k=1}^{\mathrm{n_{el}}} R_k^D(e).$$

It is worth mentioning that, while the global error quantities are equal in all the representations, the local quantities $\ell_k^{\mathscr{O}}(e)$, $a_k(e, \varepsilon)$, $R_k^P(\varepsilon)$ and $R_k^D(e)$ represent different elementary contributions to the error and, besides, they are not necessarily positive nor even real numbers.

From the four possible representations of the linear contribution of the error $\ell^{\mathscr{O}}(e)$, in this work only the two expressions involving the primal and adjoint residuals are used, thus yielding the global estimates

$$\eta^{\varepsilon} := R^P(\varepsilon^*) \quad \text{and} \quad \eta^{e} := R^D(e^*), \tag{14}$$

and its associated local error indicators $\eta_k^{\varepsilon} := R_k^P(\varepsilon^*)$ and $\eta_k^{e} := R_k^D(e^*)$, such that

$$\eta^{\varepsilon} = \sum_{k=1}^{\mathrm{n_{el}}} \eta_k^{\varepsilon} \quad \text{and} \quad \eta^{e} = \sum_{k=1}^{\mathrm{n_{el}}} \eta_k^{e}. \tag{15}$$

Remark 3 The local elemental contributions η_k^{ε} and η_k^{e} are the natural decomposition of the estimates η^{ε} and η^{e} to the elements. However, the computation of the local contributions η_k^{ε} and η_k^{e} requires the computation of local integral

forms. This can be done either by storing the elemental contributions to the system matrices and vectors or by recomputing these contributions in an elementary loop. A cheaper and more natural to implement alternative is to decompose the estimates η^ε and η^e into nodal contributions. This is because it uses the finite element nature of the estimates η^ε and η^e. In practice, the estimates e^* and ε^* are computed in a finer reference mesh associated with the space $\mathscr{V}_h$, namely $e^* = \sum_j e_j^* \phi_{h,j}$ and $\varepsilon^* = \sum_j \varepsilon_j^* \phi_{h,j}$, where $\phi_{h,j}$ are the shape functions associated with the nodes of the reference mesh, $\mathbf{x}_{h,j}$. Thus, a natural decomposition of the estimates η^ε and η^e into nodal contributions on the reference mesh holds

$$\eta^\varepsilon = \sum_j \varepsilon_j^* R^P(\phi_{h,j}) =: \sum_j \eta^\varepsilon_{\mathbf{x}_{h,j}}$$

and

$$\eta^e = \sum_j e_j^* R^D(\phi_{h,j}) =: \sum_{j=1} \eta^e_{\mathbf{x}_{h,j}}.$$

Note that $\eta^\varepsilon_{\mathbf{x}_{h,j}}$ and $\eta^e_{\mathbf{x}_{h,j}}$ are readily computed multiplying the j-th components of the finite element vectors associated to ε^* and $R^P(\cdot)$ and e^* and $R^D(\cdot)$ respectively.

Then, the local elemental contributions associated to the element Ω_k of the coarse mesh are computed from a weighted average of the local nodal contributions $\eta^\varepsilon_{\mathbf{x}_{h,j}}$ and $\eta^e_{\mathbf{x}_{h,j}}$ associated to the nodes $\mathbf{x}_{h,j}$ belonging to Ω_k. To be specific

$$\eta^\varepsilon = \sum_j \eta^\varepsilon_{\mathbf{x}_{h,j}} = \sum_{k=1}^{\mathrm{n_{el}}} \sum_{\mathbf{x}_{h,j}\in\Omega_k} \sigma_{h,j}\eta^\varepsilon_{\mathbf{x}_{h,j}} =: \sum_{k=1}^{\mathrm{n_{el}}} \hat{\eta}^\varepsilon_k, \tag{16}$$

and

$$\eta^e = \sum_j \eta^e_{\mathbf{x}_{h,j}} = \sum_{k=1}^{\mathrm{n_{el}}} \sum_{\mathbf{x}_{h,j}\in\Omega_k} \sigma_{h,j}\eta^e_{\mathbf{x}_{h,j}} =: \sum_{k=1}^{\mathrm{n_{el}}} \hat{\eta}^e_k, \tag{17}$$

where $\sigma_{h,j}$ is the inverse of the number of elements in the coarse mesh to which a particular node $\mathbf{x}_{h,j}$ belongs. For a detailed description, see [26].

A simple adaptive strategy is employed, using the local indicators produced during the calculation of the estimate for the output, to drive the non-linear output to a prescribed precision. That is, the algorithm ends if

$$\sum_{k=1}^{\mathrm{n_{el}}} \eta_k^{\circledast} + \mathscr{Q}(e^*, e^*) + \mathscr{W}(e^*) < \Delta_{\mathrm{tol}},$$

where $\eta_k^{\circledast}$ stands for any of the following local contributions η_k^ε, η_k^e, $\hat{\eta}_k^\varepsilon$ or $\hat{\eta}_k^e$, Δ_{tol} is a user-prescribed desired final accuracy, and at each level of refinement, the elements marked for refinement are those with larger values of the local linear contribution $\eta_k^{\circledast}$.

6.2 Remeshing criterion

In acoustic problems, the local contributions are not necessarily positive and in fact, in contrast to what occurs in thermal or elasticity problems, they can be complex numbers. To select the elements with larger local contributions, the modulus of the values $\eta_k^{\circledast}$ is considered, and the elements selected to be refined are the ones verifying

$$|\eta_k^{\circledast}| \geq \frac{\sum_{k=1}^{\mathrm{n_{el}}} |\eta_k^{\circledast}|}{\mathrm{n_{el}}}. \tag{18}$$

Note that this marking algorithm aims at obtaining elements with equal local error contribution. However, this is not equivalent to obtaining a uniform spatial error distribution, since the elements with larger area are penalized. In order to obtain a uniform spatial error distribution, the local contributions are weighted by the element area yielding the following marking criterion: the elements to be subdivided are the ones verifying

$$\frac{|\eta_k^{\circledast}|}{\mathrm{A}_k} \geq \frac{\sum_{k=1}^{\mathrm{n_{el}}} |\eta_k^{\circledast}|}{\mathrm{A}_\Omega}, \tag{19}$$

where A_k is the area of the element Ω_k and A_Ω is the area of the whole domain Ω. Note that expressions (18) and (19) are equivalent in uniform meshes where all the elements have the same area since in this case $\mathrm{A}_k = \mathrm{A}_\Omega/\mathrm{n_{el}}$ is constant.

7 Numerical examples

The performance of the estimates and error indicators described above is illustrated in three numerical examples. The quantities of interest are expressed as linear and quadratic functionals of the solution u. In particular, three different engineering outputs are considered. The first output is the integral of the solution over a subdomain $\Omega^{\mathscr{O}} \subset \Omega$

$$J_1(u) = \int_{\Omega^{\mathscr{O}}} u \, d\Omega, \tag{20}$$

that is, the data entering in (7) are $g^{\mathscr{O}} = \beta^{\mathscr{O}} = 0$ and $f^{\mathscr{O}} = 1$ in $\Omega^{\mathscr{O}}$ and $f^{\mathscr{O}} = 0$ elsewhere. Since the output depends linearly on u, $\ell_1^{\mathscr{O}}(v) = J_1(v)$ and $\mathscr{Q}_1(v, v) = \mathscr{W}_1(v) = 0$ in (5). Note that eventually $\Omega^{\mathscr{O}}$ can be Ω to compute an average of the solution over the whole domain.

The second output is the average of the squared modulus of the solution over a boundary strip $\Gamma^{\mathscr{O}} \subset \Gamma_N \cup \Gamma_R$

$$J_2(u) = \frac{1}{l_{\Gamma^{\mathscr{O}}}} \int_{\Gamma^{\mathscr{O}}} u\bar{u} \, d\Gamma, \tag{21}$$

where $l_{\Gamma^{\mathscr{O}}}$ is the length of the boundary strip. Since this output depends quadratically on u, $\mathscr{W}_2(v) = 0$ and the linear

and quadratic contributions are

$$\ell_2^{\mathscr{O}}(v) = \frac{1}{l_{\Gamma^{\mathscr{O}}}} \int_{\Gamma^{\mathscr{O}}} (u_H \bar{v} + \bar{u}_H v)\, d\Gamma \quad \text{and} \quad \mathscr{Q}_2(v, v) = J_2(v).$$

Indeed, appealing to (5)

$$\begin{aligned} J_2(u_H + v) &= \frac{1}{l_{\Gamma^{\mathscr{O}}}} \int_{\Gamma^{\mathscr{O}}} (u_H + v)(\overline{u_H + v})\, d\Gamma \\ &= \frac{1}{l_{\Gamma^{\mathscr{O}}}} \int_{\Gamma^{\mathscr{O}}} (u_H \bar{u}_H + u_H \bar{v} + v \bar{u}_H + v \bar{v})\, d\Gamma \\ &= J_2(u_H) + \frac{1}{l_{\Gamma^{\mathscr{O}}}} \int_{\Gamma^{\mathscr{O}}} (u_H \bar{v} + \bar{u}_H v)\, d\Gamma + J_2(v). \end{aligned}$$

It is worth noting that the linear functional $\ell_2^{\mathscr{O}}(\cdot)$ is not expressed in the form of (7). Although this functional may be used as r.h.s. for the adjoint problem (8), noting that $\ell_2^{\mathscr{O}}(v)$ is a real number coinciding with

$$\ell_2^{\mathscr{O}}(v) = 2\Re\mathrm{e}\left(\frac{1}{l_{\Gamma^{\mathscr{O}}}} \int_{\Gamma^{\mathscr{O}}} \bar{u}_H v\, d\Gamma \right),$$

allows defining the adjoint problem with respect to the auxiliary linear functional $\int_{\Gamma^{\mathscr{O}}} \bar{u}_H v\, d\Gamma / l_{\Gamma^{\mathscr{O}}}$ which corresponds to $f^{\mathscr{O}} = 0$, $\beta^{\mathscr{O}} = \bar{u}_H / l_{\Gamma^{\mathscr{O}}}$ on $\Gamma^{\mathscr{O}} \cap \Gamma_R$ and zero elsewhere and $g^{\mathscr{O}} = \bar{u}_H / l_{\Gamma^{\mathscr{O}}}$ on $\Gamma^{\mathscr{O}} \cap \Gamma_N$ and zero elsewhere.

The third output is the normalized squared $\mathscr{L}^2$-norm of the solution over a region $\Omega^{\mathscr{O}}$

$$J_3(u) = \frac{1}{A_{\Omega^{\mathscr{O}}}} \int_{\Omega^{\mathscr{O}}} u \bar{u}\, d\Omega \tag{22}$$

where $A_{\Omega^{\mathscr{O}}}$ stands for the area of the subdomain $\Omega^{\mathscr{O}}$. Again, since the output is quadratic, $\mathscr{W}_3(v) = 0$ and

$$\ell_3^{\mathscr{O}}(v) = \frac{1}{A_{\Omega^{\mathscr{O}}}} \int_{\Omega^{\mathscr{O}}} (u_H \bar{v} + \bar{u}_H v)\, d\Omega \quad \text{and} \quad \mathscr{Q}_3(v, v) = J_3(v).$$

The derivation is analogous to the one provided for $J_2(\cdot)$ except for the integrals being placed over a subdomain of Ω instead of a part of its boundary. As in the second output, the adjoint problem is defined with respect to the modified functional $\int_{\Omega^{\mathscr{O}}} \bar{u}_H v\, d\Omega / A_{\Omega^{\mathscr{O}}}$, for which the data entering in (7) are $g^{\mathscr{O}} = \beta^{\mathscr{O}} = 0$ and $f^{\mathscr{O}} = \bar{u}_H / A_{\Omega^{\mathscr{O}}}$ in $\Omega^{\mathscr{O}}$ and $f^{\mathscr{O}} = 0$ elsewhere.

Remark 4 The second and third outputs $J_2(u)$ and $J_3(u)$ are real quantities since they only involve the squared modulus of the solution. In particular, all the involved functionals, are real functions of a single complex variable, that is, for instance $\ell_2^{\mathscr{O}} : \mathbb{C} \to \mathbb{R}$. As mentioned above, in this case, the adjoint problem is defined with respect to an auxiliary non-real linear functional output. The original linear functional (and all the required estimates and local indicators) is recovered from this auxiliary functional taking the real part and multiplying by a factor two.

When reporting the numerical results, $\eta^{\varepsilon}_{\mathrm{pol}} = R^P(\varepsilon^*_{\mathrm{pol}})$, $\eta^{\varepsilon}_{\mathrm{exp}} = R^P(\varepsilon^*_{\mathrm{exp}})$, $\eta^{e}_{\mathrm{pol}} = R^D(e^*_{\mathrm{pol}})$ and $\eta^{e}_{\mathrm{exp}} = R^D(e^*_{\mathrm{exp}})$ denote the estimates of the linear contribution to the error in the quantity of interest $\eta := \ell^{\mathscr{O}}(e)$ obtained by using the post-processing strategy described in [24,25]. The subindices exp and pol indicate the kind of approximation used in the least squares fitting: either polynomial both for the real and imaginary part of the solution or a complex-exponential fitting (polynomial fitting for the logarithm of the modulus and for the angle). In order to see how well the estimators perform, the value of the true error $J(u) - J(u_H)$ or $\ell^{\mathscr{O}}(e)$ are required, but the analytical solutions of the considered problems are not available. An accurate value for the true error is obtained by making use of a sufficiently accurate approximation u_h of u in a finer reference mesh, that is, the estimates are compared with the reference values $J(u_h) - J(u_H)$ and $\eta_h := \ell^{\mathscr{O}}(e_h)$ respectively.

Note that the reference value η_h can also be recovered from a faithful representation of the adjoint problem ψ_h since $\eta_h = \ell^{\mathscr{O}}(e_h) = R^P(\psi_h) = R^P(\varepsilon_h)$. In the examples, the approximations u^* and ψ^* used to recover the estimates of the errors $e^* = u^* - u_H$ and $\varepsilon^* = \psi^* - \psi_H$ and its corresponding estimates for the output $\eta^e = R^D(e^*)$ and $\eta^{\varepsilon} = R^P(\varepsilon^*)$, are also computed using the same reference mesh. Noting that $\eta_h = R^D(e_h) = R^P(\varepsilon_h)$ reveals that the quality of the estimates depends on the quality of the approximations $e^* \approx e_h$ and $\varepsilon^* \approx \varepsilon_h$. The accuracy of these approximations is closely related to the so-called pollution or dispersion error. Since the approximations u^* and ψ^* are constructed using a constrained least-squares technique, the estimates for the error e^* and ε^* vanish at the nodes of the coarse mesh, yielding crude approximations if the solutions present large dispersion errors. In the examples, the influence of the dispersion error in the estimates for the quantity of interest is analyzed using the estimates for the dispersion error introduced in [24,25]. These estimates are denoted by E^e and E^{ε} for the primal and adjoint problems respectively. A detailed description of the computation of these estimates is given in [25].

7.1 Square with obstacle

The first example is the scattering of a plane wave by a rigid obstacle introduced in [12]. The incident wave travels in the negative y-direction inside a square domain which contains a rigid body, see Fig. 1.

The solution of the problem is composed of a prescribed incident wave plus a scattered wave, $u = u_r + u_i$, where u_r and u_i are the so-called reflected and incident waves

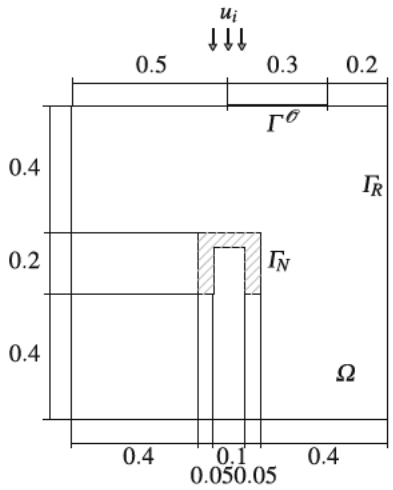

Fig. 1 Example 1: Description of the geometry and boundary conditions for the plane wave scattering by a rigid body

respectively. The incident wave is of the form $u_i = e^{i\kappa(\cos\alpha x+\sin\alpha y)}$, where κ is the wave number and $\alpha = \pi/2$ is the incident wave direction. To reproduce the scattering nature of the problem, no essential boundary conditions are imposed and it is assumed that there are no sources in the domain, $f = 0$ in Eq. (1), and that the rigid obstacle is perfectly reflecting. This is, $\nabla u \cdot \mathbf{n} = 0$ or, in terms of the incident wave, $\nabla u_r \cdot \mathbf{n} = -\nabla u_i \cdot \mathbf{n}$ on Γ_N. On the exterior boundary, Robin absorbing boundary conditions are applied. Thus, the reflected wave u_r is the solution of the Helmholtz equation (1) for $f = 0$ and $\Gamma_D = \emptyset$ and where the data entering in (2) are $g = -\nabla u_i \cdot \mathbf{n}$, $m = -ik$ and $\beta = 0$.

To demonstrate the dependence of the results on the wave number, two values of the wave number are considered: $\kappa = \pi$ and $\kappa = 3\pi$. Both the reflected and total waves obtained for this problem in a mesh of 9582 nodes are shown in Fig. 2.

For this problem, two different quantities are considered: the average of the reflected solution over the whole domain, that is $J_1(u_r)$ for $\Omega^{\mathcal{O}} = \Omega$, which is a linear quantity of interest, and the average of the squared modulus of the reflected solution over the boundary strip $\Gamma^{\mathcal{O}}$ depicted in Fig. 1, that is, $J_2(u_r)$, which depends quadratically on u_r.

The behavior of the estimates for the linear quantity of interest $J_1(u_r)$ is first analyzed for a uniform mesh refinement in a series of unstructured triangular meshes for the value $\kappa = \pi$. Three triangular meshes are considered, starting from an initial mesh of 636 nodes and obtaining the subsequent meshes by refining each triangle into four new ones, see Fig. 3.

The finite element approximation of the adjoint solution computed at the final mesh of the refinement procedure of 9582 nodes is shown in Fig. 4.

Table 1 shows the estimates obtained for the error in the quantity of interest $J_1(u_r)$. Since the quantity of interest is linear, in this case, the estimates coincide with those for the linear term. Thus, the estimates given by the different error representations (14) are compared with the reference value η_h. For each coarse mesh, the reference value is obtained by computing and approximation u_h of u in a finer mesh (each element of the coarse mesh is subdivided into 16 new ones which corresponds to $h = H/4$). Also the table shows the estimates for the dispersion error for the primal and adjoint problem E^e and E^ε respectively.

As can be seen, the estimates for the error in the quantity of interest underestimate the reference value both for the polynomial and exponential fitting. However, as reported in [25] the exponential fitting provides better results, although in this example the improvement is not that substantial when compared to the reference value. The estimates for the dispersion error are also shown in the table. Looking at the dispersion errors provided by the exponential fitting, the dispersion for the primal problem ranges from a 28% for the first mesh to a 5% for the final mesh and for the adjoint problem are below 0.3% in all the meshes. Although the dispersion is larger in the primal problem, for both problems the ratio $\kappa h_{\max} \ll 1$, in fact in average, $\kappa h_{\text{ave}} = 0.08$, 0.04 and 0.02. This explains that, although the dispersion error is significantly smaller in the adjoint problem, the difference between quality of the representations η^ε with respect to η^e are only slightly better. Indeed, since all the meshes properly satisfy the rule of thumb, the dispersion error is negligible in front of the errors appearing from the singular nature of the solution. The main source of error for this problem is not the dispersion error, and thus, even though the dispersion is smaller in the adjoint problem, the estimate ε^* does not provide a much better approximation of ε_h than e^* is of e_h. In fact, it is worth noting that most of the estimated dispersion errors are negative, yielding to finite element solutions with associated numerical wave number larger wave number than κ, differing from the predicted behavior given by a-priori estimates. This phenomena only appears when dispersion is not relevant for the problem at hand. When dispersion errors are important, the finite element method behaves as predicted by the a-priori estimates providing approximations with associated numerical wave number smaller than κ.

Figure 5 shows the local elementary contributions to the error in the quantity of interest for the initial mesh of 636 nodes. Both the local contributions of the reference values η_h^ε and η_h^e and its estimates (obtained using the polynomial and the exponential fitting) computed using the representations given in Remark 3, Eqs. (16) and (17), are shown. Note that even though the global error quantities η_h^ε and η_h^e are equal, they represent different elementary contributions to the error. The spatial distribution of the estimates is in good agreement with the reference ones: they properly detect the elements with larger contributions to the error even though the obtained elemental contributions underestimate its reference value.

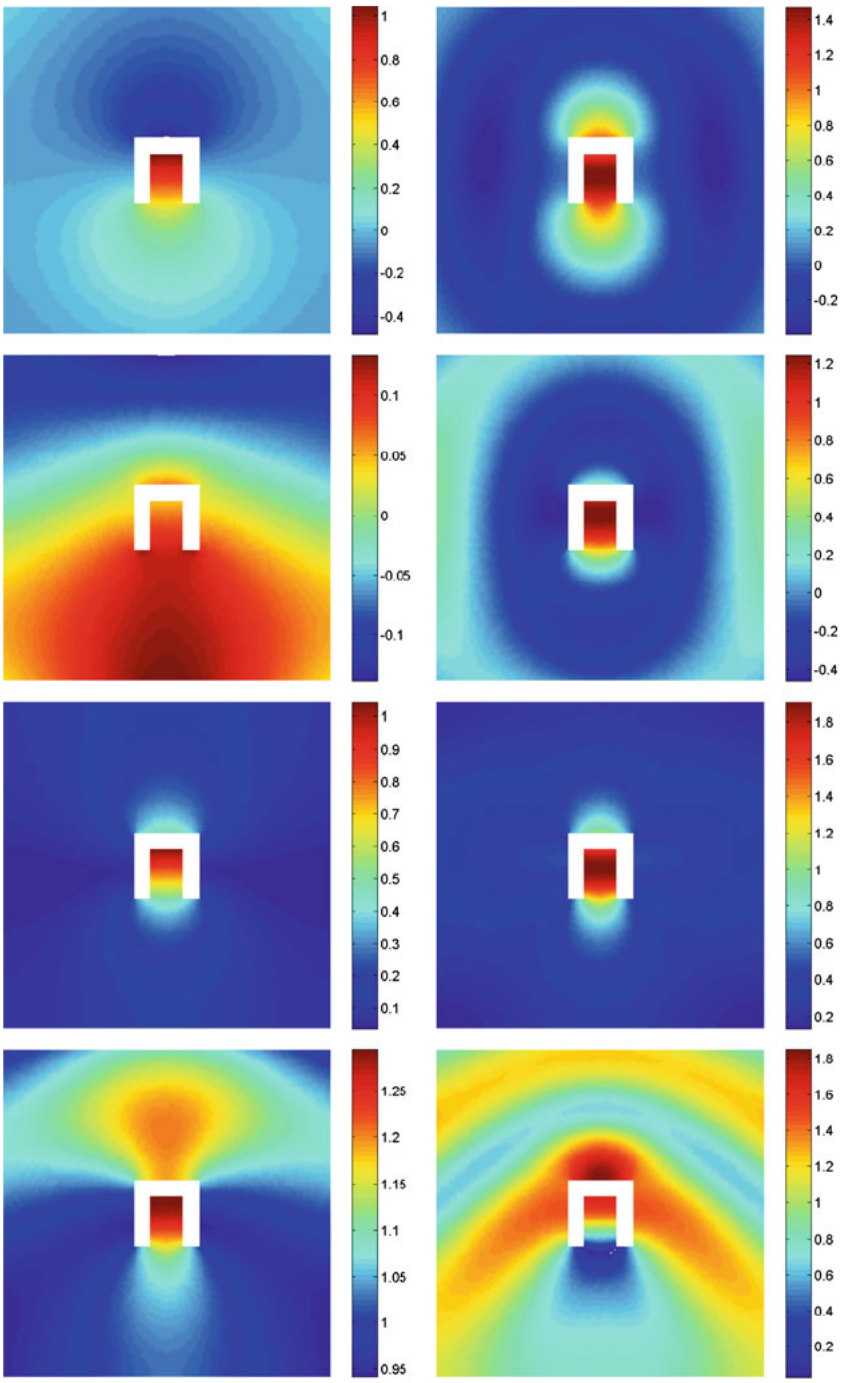

Fig. 2 Example 1: Real part (*top*), imaginary part (*middle top*) and modulus of the scattered solution u_r (*middle bottom*), that is, $\Re\mathrm{e}(u_r)$, $\Im\mathrm{m}(u_r)$ and $|u_r|$, and modulus of the total solution $|u|$ (*bottom*) for $\kappa = \pi$ (*left*) and $\kappa = 3\pi$ (*right*), computed using the Galerkin method and a mesh of 9582 nodes

The local contributions obtained using the natural restriction of the global estimates to the elements given in Eq. (15) are also shown in Fig. 6 for η_h^ε, $\eta_{\mathrm{pol}}^\varepsilon$ and $\eta_{\mathrm{exp}}^\varepsilon$. Again, although the global values coincide with those computed distributing the nodal contributions over the elements, the obtained local distributions is not the same. As can be seen, the use of the easier and cheaper to compute local contributions described in Remark 3 provides fairly good approximations to the natural restriction of the global quantities to the elements, yielding a nearly equivalent distribution of elements to be refined in the adaptive procedure. In this example, the natural decomposition yields higher values of the modulus of the elementary contributions $|\eta_k|$ since the local distribution presents larger positive and negative contributions η_k in neighboring elements. The averaging involved in the nodal-to-element representation, smoothes out these larger values yielding a more uniform distribution. Henceforth in this example, all the local contributions shown in the numerical examples are computed using the nodal-to-element representation instead of the natural representation.

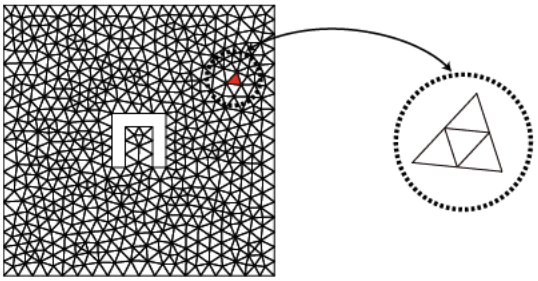

Fig. 3 Example 1: Initial mesh of 636 nodes and subdivision of each *triangle* into four new ones for the uniform mesh refinement

Figure 7 shows the elements with larger values of the estimates weighted by its area, $|\eta_k^{\circledast}|/\mathrm{A}_k$. In particular, the elements marked for refinement if 1, 5, 10 and 25% of the total elements are refined are shown respectively. Although the estimates underestimate the reference value for the error, they provide good information to guide the adaptive procedures.

The convergence of the estimates is shown in Fig. 8. Two refinement strategies are implemented: first, the meshes are uniformly refined whereby each triangle is subdivided into four sub-triangles at each step and second, the meshes are adaptively refined using the criterion given in Eq. (19). The singular nature of the solution yields an order of convergence for the uniform mesh refinement of $\mathcal{O}(H^{4/3})$ for the quantity of interest, which is equivalent to $\mathcal{O}(\mathrm{n_{np}}^{-2/3})$ where $\mathrm{n_{np}}$ denotes the number of nodes of the mesh, instead of the standard convergence rate of $\mathcal{O}(H^4)$ obtained for regular solutions. As expected, the use of an adaptive refinement strategy leads to a faster reduction of the error in the quantity of interest than if a uniform refinement is used. Again it can be seen that, in this example, all the estimates provide similar results providing an underestimation of the reference values. For comparison, the adaptive algorithm guided by the reference errors η_h^e and η_h^ε are also run. Comparing the convergence curves obtained for these two local indicators and the ones produced by the estimates, it can be seen that the estimates perform optimally since they lead to even slightly better convergence ratios than the reference errors.

The series of adapted meshes produced by the local indicator associated to $\eta_{\mathrm{exp}}^\varepsilon = R^P(\varepsilon_{\mathrm{exp}}^*)$ subdividing at each remeshing step the elements satisfying the criterion given by Eq. (19) are shown in Fig. 9. The adaptive procedure is started from the initial mesh shown in Fig. 3 and produces six new adapted meshes. The meshes obtained using the other local error indicators are virtually identical and are therefore not shown. Since the quantity of interest is the non-weighted average of the solution over the whole domain, the meshes are

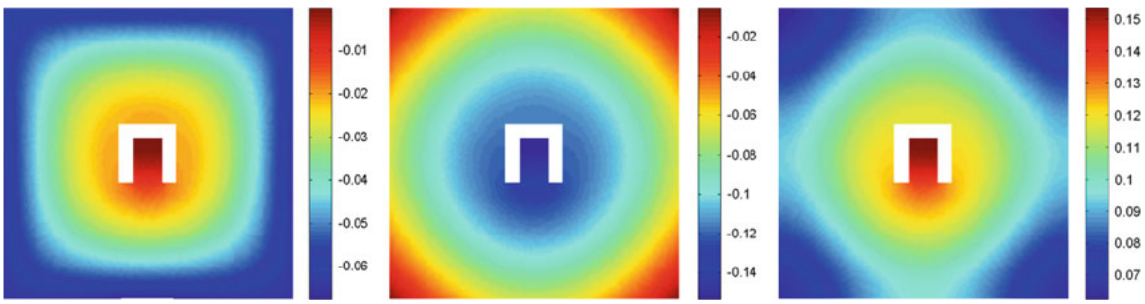

Fig. 4 Example 1: Real part (*left*), imaginary part (*middle*) and modulus (*right*) of the adjoint solution associated to the first quantity of interest $J_1(u_r)$ for $\kappa = \pi$ computed using the Galerkin method and a mesh of 9582 nodes

Table 1 Example 1: Estimates for the error in the linear quantity of interest $J_1(u_r) = \ell_1^{\mathcal{O}}(u_r)$

	Number of nodes		
	636 $\kappa h_{\max} = 0.18$	2445 $\kappa h_{\max} = 0.09$	9582 $\kappa h_{\max} = 0.05$
η_h	5.06e−4 + 7.90e−4i	2.04e−4 + 3.09e−4i	8.14e−5 + 1.22e−4i
$\eta_{\mathrm{pol}}^\varepsilon$	2.78e−4 + 5.41e−4i	1.03e−4 + 1.79e−4i	3.93e−5 + 6.23e−5i
$\eta_{\mathrm{exp}}^\varepsilon$	3.49e−4 + 5.68e−4i	1.12e−4 + 1.85e−4i	4.00e−5 + 6.22e−5i
η_{pol}^e	2.32e−4 + 4.44e−4i	9.76e−5 + 1.68e−4i	3.82e−5 + 6.02e−5i
η_{exp}^e	2.72e−4 + 5.31e−4i	1.02e−4 + 1.77e−4i	3.92e−5 + 6.21e−5i
$E_{\mathrm{pol}}^\varepsilon$	−3.17e−2	−3.25e−3	7.93e−4
$E_{\mathrm{exp}}^\varepsilon$	−9.33e−3	1.84e−3	−3.43e−4
E_{pol}^e	−1.34e+0	−4.08e−1	−1.26e−1
E_{exp}^e	−8.95e−1	−3.15e−1	−1.50e−1

The table shows the reference value for the error in the quantity of interest η_h along with its different estimates. Also, the estimated dispersion error associated to the primal and adjoint problems are given, namely $E_{\mathrm{pol}}^\varepsilon$ and E_{exp}^e

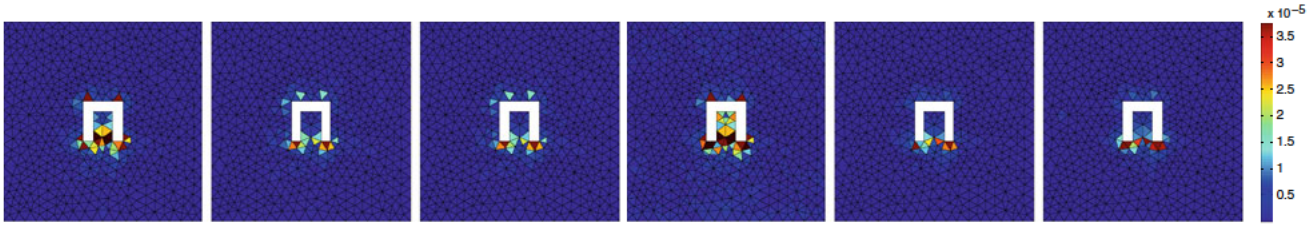

Fig. 5 Example 1: Local maps of the error in the linear quantity of interest $J_1(u_r)$. The three distributions on the *left* are obtained using the representation η^{ε}, that is, form *left* to *right*, in the first three figures η_h^{ε} (*left*), $\eta_{\text{pol}}^{\varepsilon}$ (*middle*) and $\eta_{\text{exp}}^{\varepsilon}$ (*right*) are shown. The three distributions on the *right* correspond to η^{e}, that is, η_h^{e} (*left*), η_{pol}^{e} (*middle*) and η_{exp}^{e} (*right*) are shown

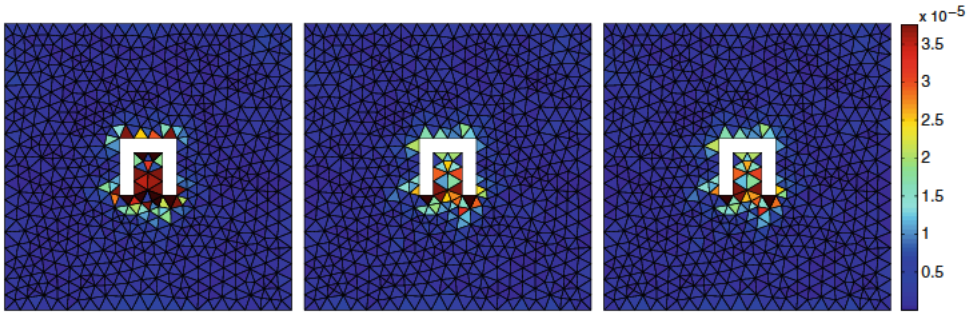

Fig. 6 Example 1: Local maps of the error in the linear quantity of interest $J_1(u_r)$ computed using the restrictions of the integrals over the elements (15). The distributions are obtained using the integral representation η^{ε}, that is, η_h^{ε} (*left*), $\eta_{\text{pol}}^{\varepsilon}$ (*middle*) and $\eta_{\text{exp}}^{\varepsilon}$ (*right*) are shown

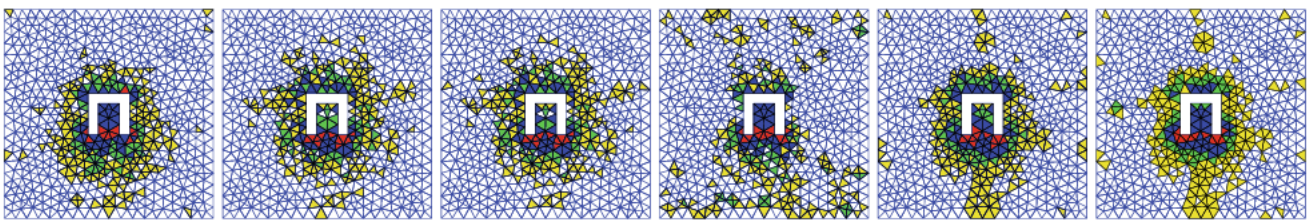

Fig. 7 Example 1: Elements marked for refinement if 1% (*red*), 5% (*red+blue*), 10% (*red+blue+green*) and 25% (*red+blue+green+yellow*) of the total elements are refined. The elements are selected using the local maps of the error in the linear quantity of interest $J_1(u_r)$ given in Fig. 5, namely from *left* to *right*: η_h^{ε}, $\eta_{\text{pol}}^{\varepsilon}$, $\eta_{\text{exp}}^{\varepsilon}$, η_h^{e}, η_{pol}^{e} and η_{exp}^{e}

refined in the areas where the primal solution presents larger errors, that is, at the neighborhood of the obstacle where the singularities occur.

The performance of the estimates is also studied for the non-linear quantity of interest $J_2(u_r)$. Figure 10 shows the finite element approximation of the adjoint solution computed using a finite element mesh of 9582 nodes for the two wave numbers $\kappa = \pi$ and $\kappa = 3\pi$. Recall that, the adjoint solution associated with a non-linear output is defined using its linear approximation, and in this case, the r.h.s. of the adjoint problem (8) is given by the auxiliary linear functional $\int_{\Gamma^{\mathscr{O}}} \bar{u}_H v \, d\Gamma / l_{\Gamma^{\mathscr{O}}}$. Thus, the adjoint solution varies for each finite element approximation u_H and the adjoint solution shown in Fig. 10 only corresponds to the adjoint problem associated to the finite element approximation u_H computed using the mesh of 9582 nodes.

In order to illustrate the influence of the different terms contributing to the error in the quantity of interest, the linear

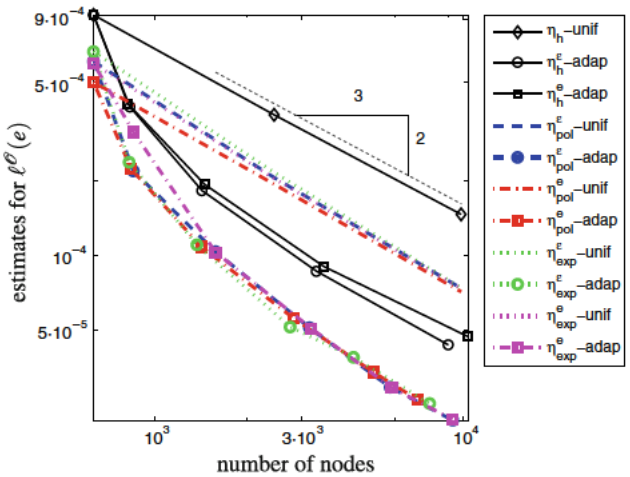

Fig. 8 Example 1: Performance of the estimators for the error in the quantity of interest $J_1(u_r)$ with a uniform and an adaptive refinement strategies. The estimates are compared with the reference values

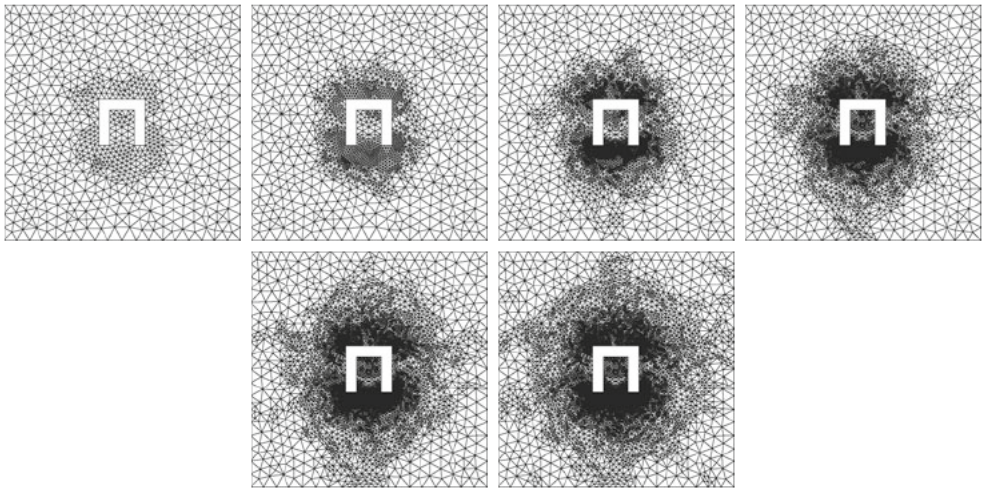

Fig. 9 Example 1: Sequence of adapted meshes obtained using the local error indicators provided by the estimate $\eta^{\varepsilon}_{\text{exp}}$ with 857, 1579, 3229, 5870, 9226 and 13852 nodes respectively, for the quantity of interest $J_1(u_r)$

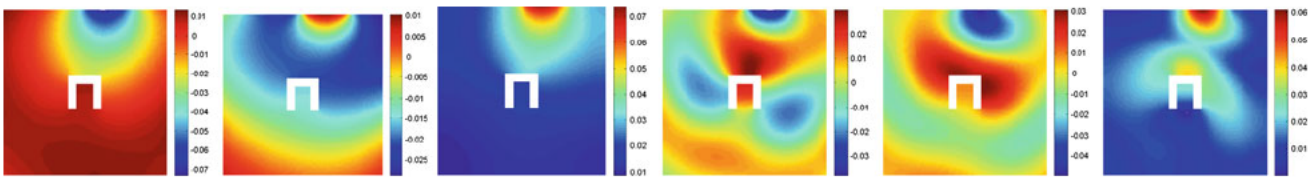

Fig. 10 Example 1: Adjoint solution associated to the second quantity of interest $J_2(u_r)$ computed using the Galerkin method and a mesh of 9582 nodes. The three figures on the *left* correspond to the real part (*left*), imaginary part (*middle*) and modulus (*right*) of the solution for $\kappa = \pi$ and the three figures on the right correspond to the real part (*left*), imaginary part (*middle*) and modulus (*right*) of the solution for $\kappa = 3\pi$. The adjoint problem is defined with respect to the auxiliary functional $\int_{\Gamma_\sigma} \bar{u}_H v \, d\Gamma / l_{\Gamma_\sigma}$

and quadratic contributions to the error along with the "full" error are shown separately for the parameter $\kappa = \pi$ (Table 2). As predicted by the theory, the total error is guided by the linear contribution, whereas the quadratic contribution is negligible since it converges faster to zero. As occurs with the first quantity of interest $J_1(u_r)$, the rate of convergence of these two terms are not the expected since the solution is singular: the finite element approximation has a convergence rate of $\mathcal{O}(H^{2/3})$ and therefore the linear and quadratic contributions to the output converge as $\mathcal{O}(H^{4/3})$ and $\mathcal{O}(H^{8/3})$ respectively, as can be appreciated in the obtained results. The same behavior is observed when the reference values are substituted by its estimates.

Neglecting the higher order terms yields the following approximation of the reference value of the quantity of interest

$$J_2(u_h) = J_2(u_H) + \ell_2^{\mathcal{O}}(e_h) + \mathcal{Q}_2(e_h, e_h) \approx \ell_2^{\mathcal{O}}(u_H) + \ell_2^{\mathcal{O}}(e_h) = \ell_2^{\mathcal{O}}(u_H) \left(1 + \frac{\ell_2^{\mathcal{O}}(e_h)}{\ell_2^{\mathcal{O}}(u_H)}\right).$$

Thus, the relative error $\rho_h := \ell^{\mathcal{O}}(e_h)/\ell^{\mathcal{O}}(u_H)$ provides a good inside of the error in the quantity of interest. Table 3

Table 2 Example 1: Influence of the linear and quadratic terms to the total error in the nonlinear quantity of interest $J_2(u_r)$ for $\kappa = \pi$

n_{np}	$\ell_2^{\mathcal{O}}(e_h)$	$\mathcal{Q}_2(e_h, e_h)$	$J_2(u_h) - J_2(u_H)$
636	1.6572e−3	3.5279e−5	1.6925e−3
2445	6.8740e−4	5.7170e−6	6.9311e−4
9582	2.7799e−4	9.1190e−7	2.7891e−4

shows the values of the reference relative error and its corresponding estimates $\rho^{\varepsilon}_{\text{exp}} := \eta^{\varepsilon}_{\text{exp}}/\ell_2^{\mathcal{O}}(u_H)$ and $\rho^{e}_{\text{exp}} := \eta^{e}_{\text{exp}}/\ell_2^{\mathcal{O}}(u_H)$ along with the estimates for the relative dispersion error $\rho^{E^{\varepsilon}}_{\text{pol}} := E^{\varepsilon}_{\text{pol}}/\kappa$ and $\rho^{E^{e}}_{\text{pol}} := E^{e}_{\text{pol}}/\kappa$ both for $\kappa = \pi$ and for $\kappa = 3\pi$.

The results are very similar to those obtained for the first quantity of interest. The two representations for the linear part of the quantity of interest $\eta^{\varepsilon}_{\text{exp}}$ and η^{e}_{exp} corresponding to the relative values $\rho^{\varepsilon}_{\text{exp}}$ and ρ^{e}_{exp} are shown. The errors are larger for $\kappa = 3\pi$ but the estimates behave similarly: the representation using the recovered adjoint error ε^* is slightly better than the representation using the recovered primal error e^* both underestimating the reference error. Also, since the values of κh_{ave} remains below 0.25 for all the meshes,

Table 3 Example 1: Estimates for the error in the linear term $\ell_2^{\mathscr{O}}(e_h)$ relative to $\ell^{\mathscr{O}}(u_H)$ and relative dispersion error for the primal and adjoint problem for a uniformly refined set of meshes

n_{np}	ρ_h	$\rho^{\varepsilon}_{\text{exp}}$	ρ^{e}_{exp}	$\rho^{E^\varepsilon}_{\text{exp}}$	$\rho^{E^e}_{\text{exp}}$
$\kappa = \pi$					
636	0.0411	0.0210	0.0189	−0.0247	−0.2849
2445	0.0170	0.0084	0.0080	−0.0089	−0.1003
9582	0.0069	0.0034	0.0033	−0.0039	−0.0479
$\kappa = 3\pi$					
636	0.1647	0.0584	0.0436	−0.0077	−0.0368
2445	0.0840	0.0387	0.0364	−0.0028	−0.0090
9582	0.0359	0.0167	0.0164	−0.0012	−0.0041

the dispersion error is very small when compared to the errors due to the singular behavior of the solution. Note that increasing κ yields smaller negative dispersion errors since for larger κ's the numerical wave number underestimates the true value yielding positive dispersion errors.

The convergence of the estimates for a uniform and an adaptive procedure using the criterion given in Eq. (19) are shown in Fig. 11 starting with the finite element mesh shown in Fig. 3. As in the results for the first quantity of interest, the adaptive refinement leads to a faster reduction of the error and it can be seen that the local indicators associated to the estimates behave properly since the convergence curves of the estimates are in very good agreement with the reference ones. Only the estimates for the exponential fitting are shown since the polynomial fitting provide similar but slightly worst results. Comparing the results for the two different wave numbers reveals that for $\kappa = 3\pi$ there is a short range where the solution is in its pre-asymptotic stage [7,27]. Note that the curves associated to the uniform refinements initially converge with a slightly smaller rate than the asymptotic one (1/2 instead of 2/3).

Figures 12 and 13 show the meshes produced by the adaptive procedure associated to the estimate $\eta^{\varepsilon}_{\text{exp}}$. The adaptive procedure refines the neighborhood of the obstacle but also refines around the boundary strip where the solution is evaluated to compute the quantity of interest. Additionally, for $\kappa = 3\pi$, the procedure also refines the zones where the solution has a larger oscillatory behavior faraway from the obstacle.

7.2 Expansion chamber

The second example is a two-dimensional model of an expansion chamber with a perforated outlet pipe as shown in Fig. 14. The source term entering in Eq. (1) is $f = 0$, and the Neumann and Robin boundary conditions entering in Eqs. (2b) and (2c) are of the form $g = -i\rho\kappa c v_n$ and $\nabla u \cdot \mathbf{n} = i\kappa u$, respectively, where in this case the material parameters are $c = 340\,\text{m/s}$ standing for the speed of sound of the medium and $\rho = 1.225\,\text{kg/m}^3$ standing for the mass density. An acoustic excitation is imposed at the inlet of the chamber, associated to a velocity $v_n = 0.1\,\text{m/s}$, whereas the chamber is assumed to be perfectly reflecting at the outlet, that is, Robin boundary conditions are applied to the outlet

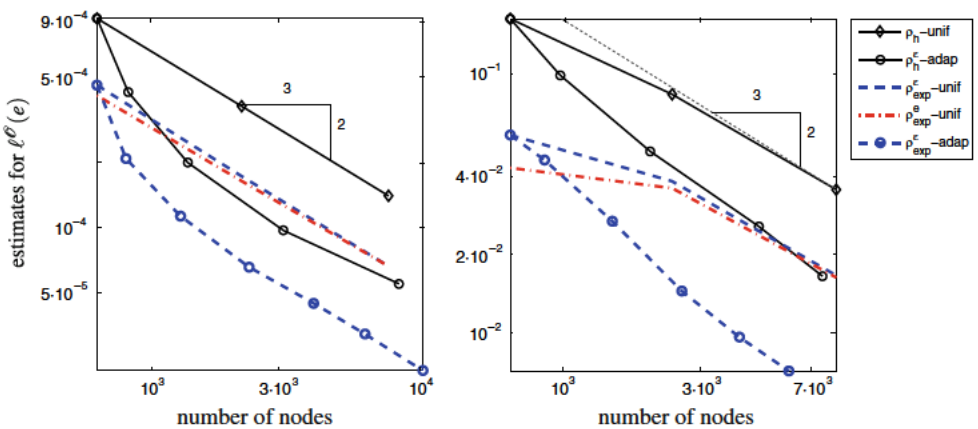

Fig. 11 Example 1: Convergence of the relative error for the quantity of interest J_2 for $\kappa = \pi$ (*left*) and $\kappa = 3\pi$ (*right*) for uniform and adaptive processes in the reference solution compared with the enhanced solutions

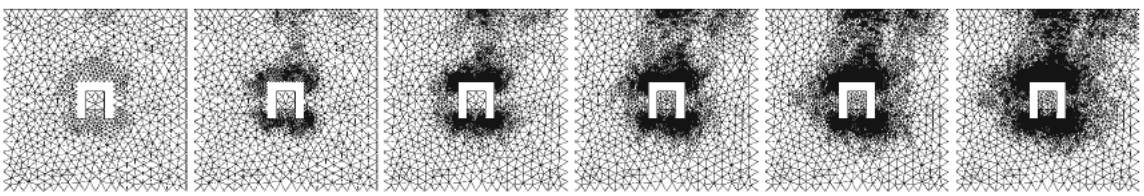

Fig. 12 Example 1: Sequence of adapted meshes with 834, 1384, 2619, 4781, 7709 and 13212 nodes, respectively. The adaptive process is driven by representation $\eta^{\varepsilon}_{\text{exp}}$, corresponding to the linear contribution $\ell_2^{\mathscr{O}}(\cdot)$ for $\kappa = \pi$

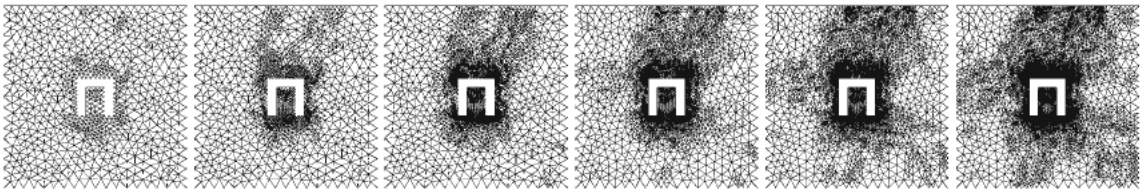

Fig. 13 Example 1: Sequence of adapted meshes with 846, 1486, 2649, 4277, 6457 and 9718 nodes. The adaptive process is driven by representation $\eta^{\varepsilon}_{\text{exp}}$, corresponding to the linear contribution $\ell_2^{\mathcal{O}}(\cdot)$ for $\kappa = 3\pi$

of the chamber. The rest of the boundary is assumed to be perfectly reflecting corresponding to $v_n = 0\,\text{m/s}$. In the computations, a wave number of $\kappa = 2\pi f/c \approx 12.936$, corresponding to a frequency of 700 Hz, has been considered.

The quantity of interest is the normalized $\mathscr{L}^2$-norm of the squared modulus of the solution over a region surrounding the outlet of the pipe, see the subdomain $\Omega^{\mathcal{O}}$ shown in Fig. 14, namely $J_3(u)$. Figures 15 and 16 show the Galerkin approximations of the primal and adjoint problems for a mesh of 1859 nodes respectively. Recall that the adjoint problem is defined using the auxiliary linear functional $\int_{\Omega^{\mathcal{O}}} \bar{u}_H v \, d\Omega / A_{\Omega^{\mathcal{O}}}$. Along with the finite element approximations, the reference solutions obtained by refining each element into 64 new ones and the reference errors are shown. The dispersion error for this mesh is one of the main sources of errors both for the primal and adjoint problem, as can be appreciated by the globally oscillating behavior of the errors.

Table 4 shows the estimates obtained for the quantity of interest $J_3(u)$ using three uniformly refined meshes, starting from the mesh shown in Fig. 17. As can be seen the estimates computed using the two proposed representations and the exponential fitting are in very good agreement with the reference values, where the reference mesh is obtained from the finite element mesh subdividing each element into 16 new ones. Also, the errors for the quantity of interest are shown, highlighting the linear term contribution. As can be seen, the linear term provides a very good inside to the total error since the quadratic term converges rapidly to zero. Since the dispersion error is an important source of error for this problem, the dispersion error is closely associated to the behavior of the representations η^{ε} and η^{e}. For the two first meshes, the dispersion error is smaller for the adjoint problem which causes the representation η^{ε} to be more accurate than η^{e}. Conversely, for the third mesh, the dispersion error is smaller for the primal problem and the representation which uses the enhanced primal error e^*, η^{e}, provide more accurate results. Thus, the dispersion error can be used to select the error representation from which to obtain the approximation for the output.

These results can also be appreciated in Fig. 18 where the estimates for the quantity of interest are depicted along with the finite element approximation and the reference value $J_3(u_h)$. Although the estimates underestimate the true error

Fig. 14 Example 2: Description of the geometry and boundary conditions for the expansion chamber

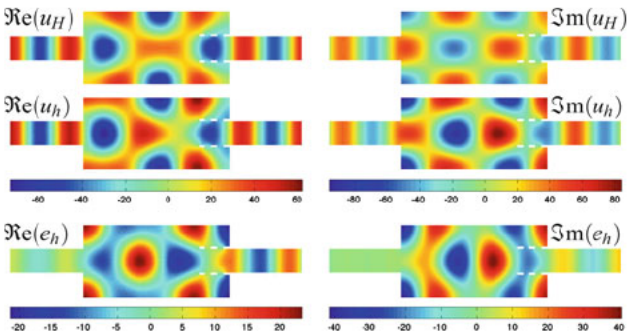

Fig. 15 Example 2: Galerkin finite element approximation of the primal problem for a mesh of 1859 nodes (*top*). The middle figures are the Galerkin approximation for a mesh obtained dividing each element into 64 new ones. The reference error with respect to this mesh is shown in the bottom

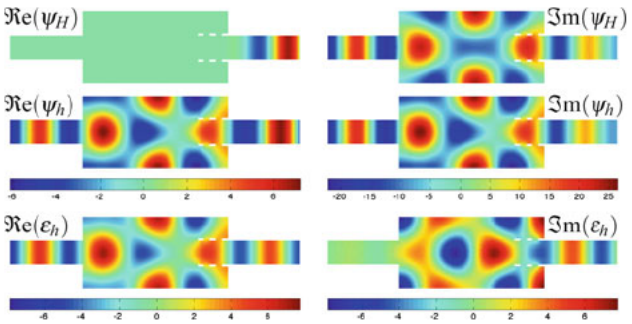

Fig. 16 Example 2: Galerkin finite element approximation of the adjoint problem for a mesh of 1859 nodes (*top*). The *middle figures* are the Galerkin approximation for a mesh obtained dividing each element into 64 new ones. The reference error with respect to this mesh is shown in the *bottom*

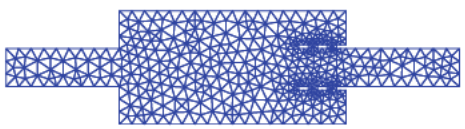

Fig. 17 Example 2: Initial mesh for the uniform and adaptive procedures of 494 nodes

Table 4 Example 2: Estimates for the non-linear quantity of interest $J_3(u)$ and for the its error, including the linear contribution to the quantity of interest and the dispersion errors for the primal and adjoint problems. The meshes are obtained by refining each element into 16 new ones

	Number of nodes		
	494	1859	7193
$J(u_h)$	2.2067e+3	2.2588e+3	2.2763e+3
$J(u_H)$	1.8796e+3	2.1128e+3	2.2067e+3
$J(u_H) + \eta^\varepsilon + \mathcal{Q}(e^*, e^*)$	2.1548e+3	2.1967e+3	2.2611e+3
$J(u_H) + \eta^e + \mathcal{Q}(e^*, e^*)$	2.1082e+3	2.1961e+3	2.2622e+3
$J(u_h) - J(u_H)$	3.2701e+2	1.4603e+2	6.9648e+1
$\eta^\varepsilon + \mathcal{Q}(e^*, e^*)$	2.7511e+2	8.3916e+1	5.4420e+1
$\eta^e + \mathcal{Q}(e^*, e^*)$	2.2854e+2	8.3293e+1	5.5533e+1
η^ε	2.7276e+2	8.3709e+1	5.4406e+1
η^e	2.2619e+2	8.3087e+1	5.5518e+1
E^ε	2.4556e−1	6.8103e−2	1.5967e−2
E^e	2.6351e−1	6.8293e−2	1.5780e−2

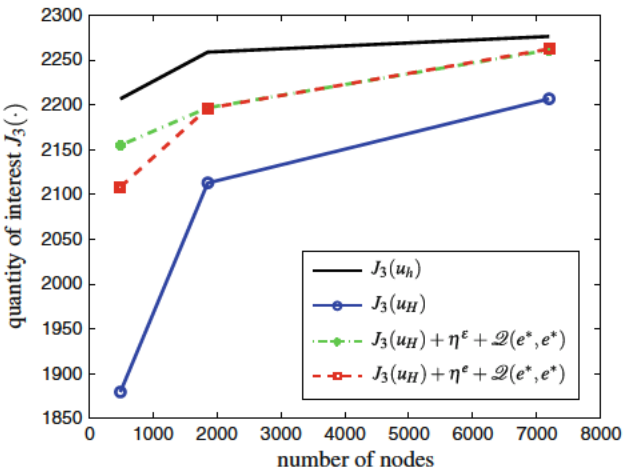

Fig. 18 Example 2: Behavior for the estimates for the quantity of interest $J_3(u)$ with respect to a uniform mesh refinement

$J_3(u)$, they provide a much better approximation to the quantity of interest than $J_3(u_H)$ with very few effort.

The behavior of the estimate η^ε and its suitability for guiding an adaptive refinement algorithm is illustrated by applying different adaptive procedures. Starting from the mesh given in Fig. 17 the following six strategies are implemented to refine the elements at each step.

- *Strategy 1:* the elements to be refined are the ones verifying criterion (18).
- *Strategy 2:* the elements to be refined are the ones verifying criterion (19).
- *Strategy 3:* at each step, 10% of the elements are refined, those with larger contributions $|\eta_k^\varepsilon|$.

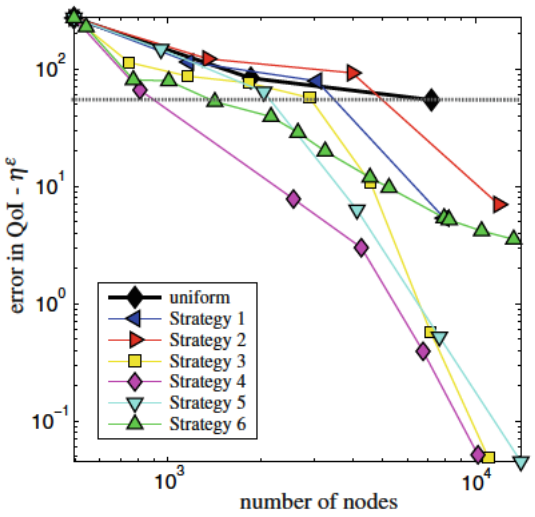

Fig. 19 Example 2: Convergence of the error in the quantity of interest for the different adaptive strategies using the local error indicators associated to η^ε

- *Strategy 4:* at each step, 10% of the elements are refined, those with larger contributions $|\eta_k^\varepsilon|/A_k$.
- *Strategy 5:* the smallest number of elements such that the sum of the contributions $|\eta_k^\varepsilon|$ toward the global error $\sum_{k=1}^{n_{el}} |\eta_k^\varepsilon|$ from these elements exceeds 25% of its value are refined.
- *Strategy 6:* all elements on which the local error estimate $|\eta_k^\varepsilon|$ exceeds 50% of the largest local error estimate are refined at each step.

The results are shown in Fig. 19.

Strategy four produces the best results, with those obtained using strategies three and five running a close second and third. The indicators based on strategies one and two produce noticeably poorer accuracy since they over refine the meshes at each step. Note that in the initial steps the behavior is similar to a uniform refinement. Penalizing the elements with smaller area provides an improvement of the accuracy as can be seen comparing strategies one and two and strategies three and four. Note also that strategies three and four yield to similar accuracies, but at the initial steps, strategy three yield poorer results since it produces nearly uniformly refined meshes. Thus, analogous strategies to five and six could be develop taking into account for the area of the elements. From the graph it is clear that using a criterion that controls the ratio of elements to be refined (preventing the possibility of a uniform refinement) produces optimal adapted meshes, that is, meshes with the least number of elements for a prescribed given accuracy. Increasing the percentages in strategies three, four and six or decreasing it in the sixth, increases the number of elements to be refined producing not so optimal meshes. Hence a compromise between number of adaptive steps and

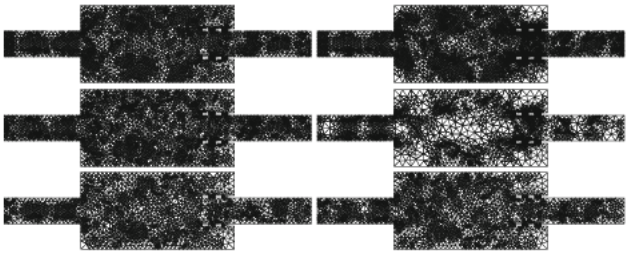

Fig. 20 Example 2: Intermediate meshes of the adaptive procedures for the six different strategies: third step of strategy 1 (*top-left*) with 3047 nodes and $\eta^{\varepsilon} = 79.11$, third step of strategy 2 (*top-right*) with 3976 nodes and $\eta^{\varepsilon} = 92.71$, fifth step of strategy 3 (*middle-left*) with 2892 nodes and $\eta^{\varepsilon} = 56.77$, second step of strategy 4 (*middle-right*) with 810 nodes with $\eta^{\varepsilon} = 66.62$, third step of strategy 5 (*bottom-left*) with 2050 nodes and $\eta^{\varepsilon} = 63.86$ and fifth step of strategy 6 (*bottom-right*) with 1005 nodes and $\eta^{\varepsilon} = 52.56$

accuracy is required. Finally, strategy six does not provide very good results in problems where the error is substantially larger in some parts of the domain. As can be seen in the figure, the ratio of convergence of this strategy is better than the ratio of a uniform refinement, but provides poorer results than other strategies. Note also that very few elements are refined in each iteration.

The intermediate meshes with precision closer to the one obtained in the second iteration of the uniform refinement procedure are shown in Fig. 20 for the six strategies. The second iteration of the uniform refinement provides a mesh of 7193 nodes and achieves a precision of $\eta^{\varepsilon} = 54.41$.

It can be observed that the meshes produced using strategies one and two tend to exhibit a more uniform refinement compared with those obtained using strategy four, which accounts for the poorer accuracy of the resulting approximation. Also, from the intermediate meshes, it can be observed that, as mentioned before, although strategies four, three and five achieve similar results for the final mesh, at the intermediate steps, joining the control of the elements to be refined along with penalizing the elements with smaller area, namely, strategy four, provides the best results. This is clearly appreciated in the intermediate meshes, where the mesh produced by strategy four is clearly more adapted to the features of the solution that all the other strategies. Adding the area factor to strategies five and six would produce similar results, although in the case of strategy 6 also a control on the minimal elements to be refined would be also advisable. It is also worth mentioning, that strategies one and two can be adapted to control the elements to be refined by introducing a constant factor into criterions (18) and (19) as follows: $|\eta_k^{\varepsilon}| \geq C \sum_{k=1}^{\mathrm{n_{el}}} |\eta_k^{\varepsilon}|/\mathrm{n_{el}}$ and $|\eta_k^{\varepsilon}|/\mathrm{A}_k \geq C \sum_{k=1}^{\mathrm{n_{el}}} |\eta_k^{\varepsilon}|/\mathrm{A}_{\Omega}$. A value of $C = 1$ corresponds to strategies one and two respectively. Note that, however, increasing the value of C does not ensure that the set of elements to be refined is a non-empty set (for instance if a uniform mesh with uniform distribution of the error is obtained).

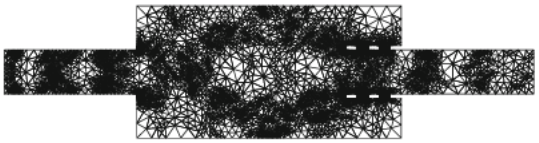

Fig. 21 Example 2: Final mesh obtained using the adaptive procedure described in strategy four with 10200 nodes

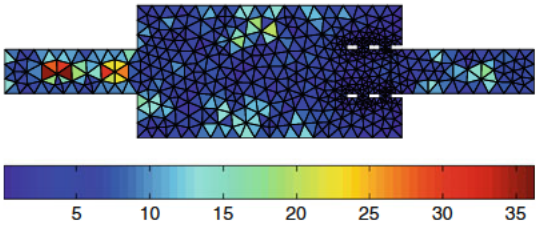

Fig. 22 Example 2: Local maps of the error in the linear term contribution to the quantity of interest $J_3(u)$ using the representation η^{ε}

The final mesh of 10200 nodes obtained using strategy four is shown in Fig. 21. Strategies three and four produce meshes with similar accuracy but with a more diffuse or uniform refinement. The predicted quantity of interest for this final mesh is $J(u) \approx 2319.1$ associated to the errors $\eta^{\varepsilon} = 0.051528$ and $\mathscr{Q}(e^*, e^*) = 0.0000375$. Again, the quadratic contribution to the error is negligible in front of the linear contribution.

Finally, Fig. 22 shows the local elementary contributions of η^{ε} to the error in the quantity of interest for the initial mesh and Fig. 23 shows the elements marked to be refined for each of the proposed adaptive strategies, reaffirming the behavior observed in the convergence curves and the intermediate meshes.

7.3 Car cavity

This example studies the noise transmission inside a two-dimensional section of the cabin of a car which is excited by vibrations of the front panel and damped by Robin boundary conditions. This example is frequently used as a benchmark problem in error assessment for interior acoustic problems [9,28,29]. The geometry of the cabin is shown in Fig. 24. The size of the domain is characterized by the maximum horizontal and vertical lengths, $L_x = 2.7\,\mathrm{m}$ and $L_y = 1.1\,\mathrm{m}$, respectively. The source term entering in Eq. (1) is $f = 0$, and the Neumann and Robin boundary conditions entering in Eqs. (2b) and (2c) are of the form $g = -i\rho c\kappa v_n$ and $mu = -i\rho c\kappa A_n u$, where in this case the material parameters are $c = 340\,\mathrm{m/s}$ and $\rho = 1.225\,\mathrm{kg/m^3}$. The vibrating front panel is excited with a unit normal velocity $v_n = 1\,\mathrm{m/s}$ whereas the roof is considered to be an absorbent panel with associated admittance $A_n = 1/2000\,\mathrm{m\ (Pa\ s)^{-1}}$. The normal boundary velocity is set to be zero at the other sides, $v_n = 0\,\mathrm{m/s}$. Finally, a wave number of $\kappa \approx 9.7$, equivalent

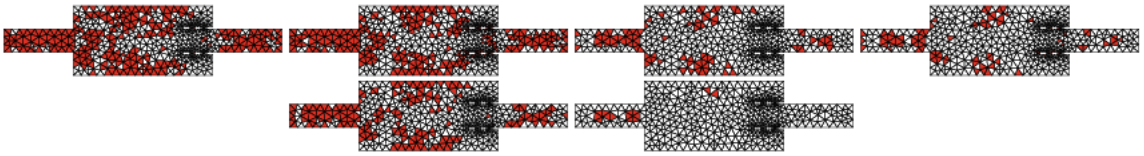

Fig. 23 Example 2: Elements to be refined in the first step highlighted for the six different strategies (from *top-left to bottom-right*): strategy 1 with 303 elements, strategy 2 with 316 elements, strategy 3 with 87 elements, strategy 4 with 87 elements, strategy 5 with 183 elements and strategy 6 with 14 elements

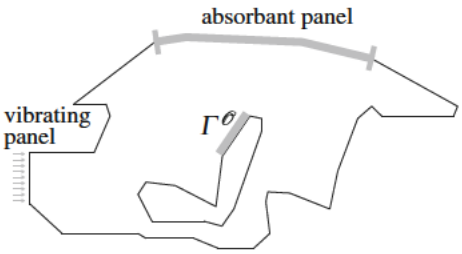

Fig. 24 Example 3: Description of the two-dimensional section of the cabin of a car and its associated boundary conditions

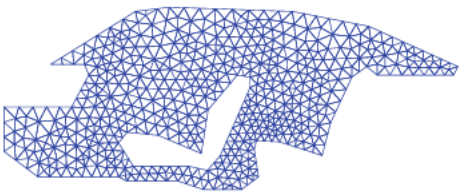

Fig. 25 Example 3: Initial mesh for the adaptive procedure with 568 nodes

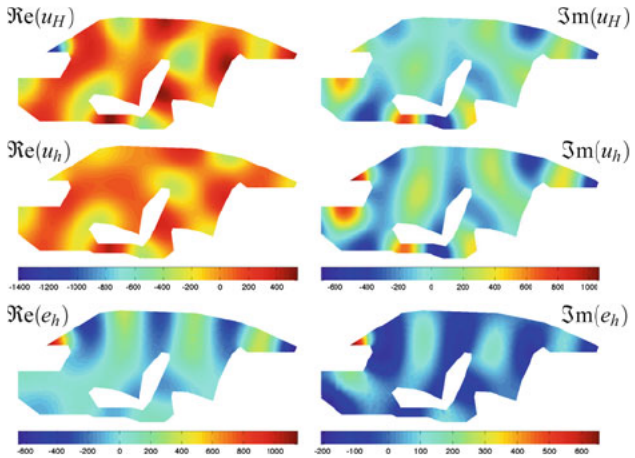

Fig. 26 Example 3: Galerkin finite element approximation of the primal problem for the initial mesh of 568 nodes (*top*). The middle figures are the Galerkin approximation for a mesh obtained dividing each element into 256 new ones. The reference error with respect to this mesh is shown in the *bottom*

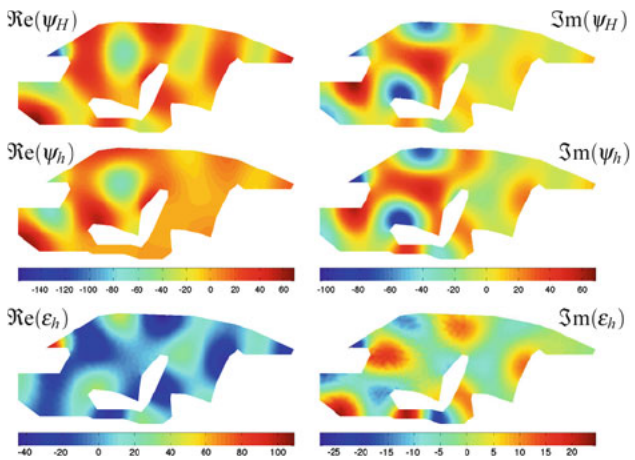

Fig. 27 Example 3: Galerkin finite element approximation of the adjoint problem for a mesh of 568 nodes (*top*). The *middle figures* are the Galerkin approximation for a mesh obtained dividing each element into 64 new ones. The reference error with respect to this mesh is shown in the *bottom*

to a frequency of 525 Hz, has been considered in the computations.

The output of interest is the average of the squared modulus of the solution over the boundary strip $\Gamma^{\mathcal{O}}$ shown in Fig. 24, namely $J_2(u)$. The initial mesh used for this example is shown in Fig. 25. Figures 26 and 27 show the Galerkin approximations of the primal and adjoint problems for the initial mesh along with the finite element approximations computed in a reference mesh obtained by refining each element into 256 new ones. The figures also show the approximation of the true errors obtained by subtracting the two finite element approximations. The dispersion errors associated to the primal and adjoint problems are $E^{\varepsilon} = 0.075$ and $E^{e} = 0.130$, respectively. Thus, the adjoint problem presents smaller dispersion errors and it is expected that in this mesh, the estimate η^{ε} provides better approximations to the error in the quantity of interest than η^{e}.

The mesh is adaptively refined using the refinement algorithm named after *strategy 2* in the previous example. In this case, an adaptive strategy producing a more uniform refinement is preferred due to the large dispersion errors present in the solutions. The adaptive procedure is guided by the indicators provided by η^{ε}. However, in each step, the estimate η^{e} is also computed to compare the results.

The initial mesh of 568 elements provides the approximation of the quantity of interest $J_2(u_H) = 27093.7$ while the error estimation procedures described in this work

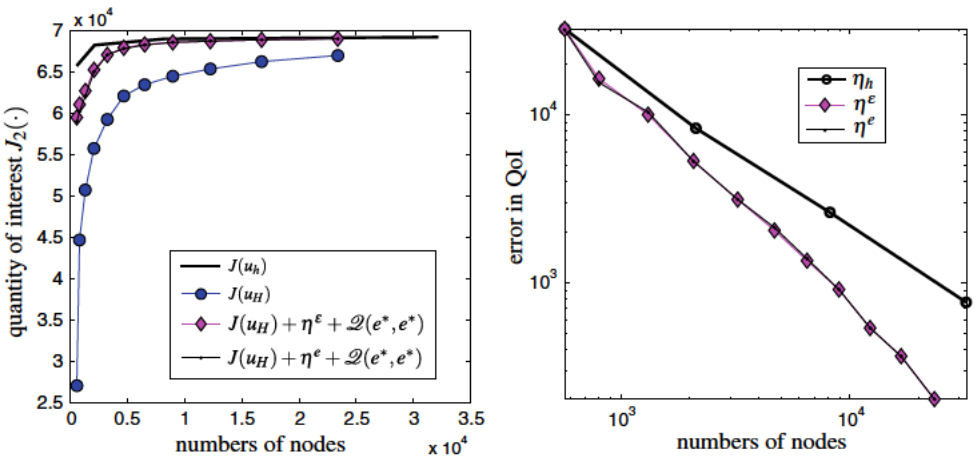

Fig. 28 Example 3: Behavior of the estimates for the nonlinear quantity of interest $J_2(u)$ (*top*) and convergence of the linear contributions to the error (*bottom*)

provide the estimates for the error in the quantity of interest $\eta^{\varepsilon} = 32461.3$, $\eta^{e} = 31966.4$ and $\mathcal{Q}(e^*, e^*) = 5.6$.

Thus, the estimates for the quantity of interest in the first mesh are $J_2(u) \approx 59560.6$ and 59065.8 for the two different representations, respectively. The reference value for the quantity of interest $J_2(u_h) = 65821.7$ confirming that, since the dispersion error is smaller in the adjoint problem, the estimate provided by η^{ε} is better than the one provided by η^{e}, although since the underestimation is quite large in both cases, both estimates produce similar accuracy of the estimates. It can also be seen that even for the initial mesh, the contribution of the quadratic term to the quantity of interest is negligible in front of the linear contribution. After remeshing, the final mesh provides the approximation for the quantity of interest $J_2(u_H) = 67076.3$ and the estimates $J_2(u) \approx 69089.6$ and 69098.1 provided by η^{ε} and η^{e} respectively. Note that in this case, since the estimates for the dispersion errors are $E^{\varepsilon} = 0.00358$ and $E^{e} = 0.00487$, the second estimates is expected to be more reliable.

The convergence of the estimates is shown in Fig. 28. As can be seen, both representations for the quantity of interest provide similar results improving the accuracy of the finite element approximation with very little computational effort (they only involve an inexpensive post-processing of the finite element solutions).

Figure 29 shows an intermediate and the final adaptively refined meshes. As can be seen, the adaptive procedure refines the corners where the solution presents larger singularities and also the front part of the mesh which is the region most affecting the quantity of interest. This is confirmed by the fact that the mesh beside the seat is only refined in the reentrant corners where the solution is singular.

The same example is considered in [9,30] where mesh adaptivity aiming at reducing global measures of the error are considered. Although the examples shown therein refer to lower wave numbers, a close comparison with the results obtained with the goal-oriented strategy presented in this work reveals that our technique properly resolves the singularities of the primal problem (refining the regions of the domain where the primal error is larger) while refining, at the same time, the areas relevant for the quantity of interest.

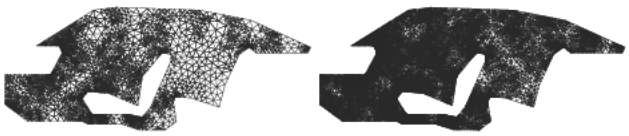

Fig. 29 Example 3: Intermediate and final meshes obtained using the adaptive process associated to strategy 4. Iteration fourth (*left*) with 3235 nodes and final with 23380 nodes

8 Conclusions

A simple and effective strategy for guiding goal-oriented adaptive procedures has been presented, based on the post-processing techniques introduced in [24,25]. Two different representations of the error in the quantities of interest have been studied which provide similar results. It has been shown that the accuracy of these representations, which involve the post-processing of either the primal or adjoint finite element approximations, is related to the dispersion error of the corresponding problems. The adaptive procedure is valid both linear and non-linear quantities of interest, but in both cases the local indicators driving the adaptivity are obtained from linearized approximations of the output. In all the analyzed examples the linear part of the quantity of interest is the leading term, since the higher order contributions converge faster to zero.

References

1. Ihlenburg F, Babuška I (1995) Dispersion analysis and error estimation of Galerkin fininite element methods for the Helmohltz equation. Int J Numer Methods Eng 38:3745–3774

2. Ihlenburg F, Babuška I (1995) Finite element solution of the Helmholtz equation with high wave number. Part 1: the *hp*-version of the FEM. Comput Math Appl 38:9–37
3. Ihlenburg F (1998) Finite element analysis of acoustic scattering. In: Applied mathematical sciences, vol 132. Springer-Verlarg, New York
4. Deraemaeker A, Babuška I, Bouillard P (1999) Dispersion and pollution of the FEM solution for the Helmholtz equation in one, two and three dimensions. Int J Numer Methods Eng 46(4):471–499
5. Babuška I, Sauter SA (2000) Is the pollution effect of the FEM avoidable for the Helmholtz equation considering high wavenumber? SIAM Rev 42(3):451–484
6. Stewart JR, Hughes TJR (1996) Explicit residual-based a posteriori error estimation for finite element discretizations of the Helmholtz equation. Computation of the constant and new measures of error estimator quality. Comput Methods Appl Mech Eng 131 (3–4):335–363
7. Babuška I, Ihlenburg F, Strouboulis T, Gangaraj SK (1997) A posterori error estimation for finite element solutions of Helmholtz' equation Part I: The quality of locar indicators and estimators. Int J Numer Methods Eng 40:3443–3462
8. Bouillard P (1999) Admissible fields and error estimation for acoustic fea with low wave numbers. Comput Struct 73(1–5): 227–237
9. Bouillard P, Ihlenburg F (1999) Error estimation and adaptivity for the finite element method in acoustics: 2d and 3d applications. Comput Methods Appl Mech. Eng 176(1):147–163
10. Irimie S, Bouillard P (2001) A residual a posteriori error estimator for the finite element solution of the Helmholtz equation. Comput Methods Appl Mech Eng 190(31):4027–4042
11. Peraire J, Patera AT (1999) Asymptotic a posteriori finite element bounds for the outputs of noncoercive problems: the Helmholtz and burgers equations. Comput Methods Appl Mech Eng 171(1): 77–86
12. Sarrate J, Peraire J, Patera AT (1999) A posteriori finite element error bounds for non-linear outputs of the Helmholtz equation. Int J Numer Methods Eng 31(1):17–36
13. Walsh T, Demkowicz T (2003) *hp* Boundary element modeling of the external human auditory system: goal oriented adaptivity with multiple load vectors. Comput Methods Appl Mech Eng 192(1–2): 125–146
14. Strouboulis T, Babuška I, Hidajat R (2006) The generalized finite element method for Helmholtz equation theory, computation, and open problems. Comput Methods Appl Mech Eng 195:4711–4731
15. Maday Y, Patera AT, Peraire J (1999) A general formulation for a posteriori bounds for output functionals of partial differential equations: application to the eigenvalue problem. C R Acad Sci Paris Anal Numér 328(1):823–828
16. Zienkiewicz O, Zhu J (1987) A simple error estimator and adaptive procedure for practical engineering analysis. Int J Numer Methods Eng 24:337–357
17. Zienkiewicz O, Zhu J (1992) The superconvergent patch recovery (SPR) and adaptive finite element refinement. Comput Methods Appl Mech Eng 101:207–224
18. Díez P, Rodenas JJ, Zienkiewicz OC (2007) Equilibrated patch recovery error estimates: simple and accurate upper bounds of the error. Int J Numer Methods Eng 69(10):2075–2098
19. Ainsworth M, Oden JT (2000) A posteriori error estimation in finite element analysis. Wiley, Chichester
20. Ladevèze P, Leguillon D (1983) Error estimate procedure in the finite element method and applications. SIAM J Numer Anal 20(3):485–509
21. Díez P, Parés N, Huerta A (2003) Recovering lower bounds of the error by postprocessing implicit residual a posteriori error estimates. Int J Numer Methods Eng 56(10):1465–1488
22. Parés N, Díez P, Huerta A (2006) Subdomain-based flux-free a posteriori error estimators. Comput Methods Appl Mech Eng 195(4–6):297–323
23. Parés N, Santos H, Díez P (2009) Guaranteed energy error bounds for the Poisson equation using a flux-free approach: solving the local problems in subdomains. Int J Numer Methods Eng 79(10):1203–1244
24. Steffens LM, Díez P (2009) A simple strategy to assess the error in the numerical wave number of the finite element solution of the Helmholtz equation. Comput Methods Appl Mech Eng 198: 1389–1400
25. Steffens LM, Parés N, Díez P (2010) Estimation of the dispersion error in the numerical wave number of standard and stabilized finite element approximations of the Helmholtz equation. Int J Numer Methods Eng. doi:10.1002/nme.3104
26. Díez P, Calderón G (2007) Remeshing criteria and proper error representations for goal oriented *h*-adaptivity. Comput Methods Appl Mech Eng 196(4–6):719–733
27. Babuška I, Ihlenburg F, Strouboulis T, Gangaraj K (1997) A posterori error estimation for finite element solutions of Helmholtz' Part II: estimation of the pollution error. Int J Numer Methods Eng 40:3883–3900
28. Suleau S, Deraemaeker A, Bouillard P (2000) Dispersion and pollution of meshless solutions for the Helmholtz equation. Comput Methods Appl Mech Eng 190:639–657
29. Harari I, Magoulès F (2004) Numerical investigations of stabilized finite element computations for acoustics. Wave Motion 39: 339–349
30. Baušys R, Hager P, Wiberg NE (2001) Postprocessing techniques and *h*-adaptive finite element-eigenproblem analysis. Comput Struct 79:2039–2052